

DESIGN OF A SWITCHED RELUCTANCE MOTOR DRIVE FOR AUTOMOTIVE APPLICATIONS

Analytical Modelling and Finite Element Validation of a 6/4 SRM

SYED HASSAN TIRMIZI

A Thesis presented for the fulfillment of the degree of
Master of Science in Sustainable Transportation of Energy and
Power Systems



Department of Electrical and Electronics Engineering
The University of Nottingham
United Kingdom
31/08/2018

Declaration of Authorship

I, Hassan Tirmizi, solemnly declare that this thesis titled, ‘Design of a Switched Reluctance Motor drive for automotive applications’ and the work presented in it are my own. I confirm that:

- This work was done wholly or mainly while in candidature for a research degree at this University.
- Where any part of this thesis has previously been submitted for a degree or any other qualification at this University or any other institution, this has been clearly stated.
- Where I have consulted the published work of others, this is always clearly attributed.
- Where I have quoted from the work of others, the source is always given. With the exception of such quotations, this thesis is entirely my own work.
- I have acknowledged all main sources of help.
- Where the thesis is based on work done by myself jointly with others, I have made clear exactly what was done by others and what I have contributed myself.

Signed: Hassan Tirmizi

Date: 31/08/2018

“Continue your quest for the attainment of knowledge and wisdom right from cradle till grave.”

Prophet Muhammad

THE UNIVERSITY OF NOTTINGHAM

Abstract

Power Electronics and Machines group
Department of Electrical and Electronics Engineering

Master of Science

Design of Switched Reluctance Motor drive for automotive applications

by [Hassan Tirmizi](#)

Switched Reluctance Machines (SRM) are a subject of renewed interest in the automotive sector owing to their viability as potential substitutes for PMSM drives. Being a rare earth magnet free machine coupled with fast torque dynamics and a robust rotor structure are the manifold advantages that SRMs offer and thus various manufacturers are exploring them as potential candidates for the Motor propulsion systems of automotive drivetrains

In this Thesis report an attempt has been made to model the SRM by framing an analytical set of equations that could describe the machine's performance in a befitting manner. The design problem posed by the manufacturer is effectively broken down into blocks of Geometry evaluation, Aligned Magnetic Circuit solution and Unaligned magnetic circuit solution. These blocks in turn output a feasible range of the design variables as a function of the machine's bore diameter based on the imposed initial constraints and chosen design parameters.

The sizing of the SRM is then achieved by mapping the flux linkage points evaluated from the aligned and the unaligned circuit configurations. The resulting Magnetic Co-Energy loop is proportional to the torque that can be developed from the SRM and the analytical results are then validated through Finite element Numerical Simulations . . .

Acknowledgements

I would like to thank my Thesis supervisor Professor Michelle Degano who supported me wholeheartedly and guided me right throughout the course of the thesis. Also i benefited immensely from the supervision of PhD student Mr Roberto Rocca. Without the efforts of these respected individuals the work presented wouldn't have been possible . . .

Contents

Declaration of Authorship	i
Abstract	iii
Acknowledgements	iv
List of Figures	viii
List of Tables	x
Abbreviations	xi
Physical Constants	xii
Symbols	xiii
1 Introduction to Switched Reluctance Machines	1
1.1 Principle of Operation	1
1.1.1 Torque Calculation using the Co-Energy method	3
1.1.2 Torque analysis using Inductance Variation	4
1.1.3 Inductance Profile	5
1.1.4 Dynamic Model of SRM	7
1.2 Advantages of Switched Reluctance Machines	8
2 Background Review of Switched Reluctance Machines	9
2.1 Inductance profile of the 6/4 SRM machine	9
2.1.1 Relationship between the flux and the rotation angle	10
2.1.2 Relationship between the flux and the current	12
2.2 Modes of Operation of the Switched Reluctance Machine	13
2.3 Control Strategy for SRM drives	14
2.3.1 SRM Low speed operation	15
2.3.2 High speed motoring operation	15
2.3.3 Control strategies for the different modes of operation	17

3	Magnetic Material	19
3.1	Salient points about the Material Selection	20
3.2	Magnetization curves of M300-35A	20
3.2.1	Estimation of SRM design Ratios	21
4	Initial Sizing of the SRM drive	23
4.1	Key considerations for the design of SRM drives	23
4.2	Design Specifications	24
4.3	Calculation of the Bore Diameter	27
4.3.1	Stator pole width	27
4.3.2	Rotor pole width	27
4.3.3	Stator yoke height	27
4.3.4	Rotor yoke height	28
4.3.5	Stator Pole height	28
4.4	Rotor Pole height evaluation	28
4.4.1	Permeance Method for Inductance Calculation	28
4.4.1.1	Region-1 of the Stator-Rotor flux path	29
4.4.1.2	Region-2 of the Stator-Rotor flux path	30
4.4.1.3	Region-3 of the Stator-Rotor flux path	31
4.4.2	Variation of the unaligned SRM inductance	32
4.5	Performance analysis of Initial Sizing Algorithm	33
5	Design of SRM using Torque Sizing Equation	36
5.1	Magnetic Co-Energy Sizing	36
5.1.1	Calculation of the peak current	36
5.1.2	Calculation of Flux linkages in the aligned position	37
5.1.3	Torque Sizing equation	37
5.2	Geometry Calculation	38
5.2.1	Rotor pole height improvement	38
5.2.2	SRM Geometrical plots	38
5.3	Aligned Magnetic Circuit Calculations	39
5.3.1	Magnetic Flux density Calculations	39
5.4	Unaligned Magnetic Circuit	42
5.4.1	Area of the Co-Energy Loop	42
5.4.2	Magnetic Co-Energy Sizing Algorithm	43
6	Conclusions and Results	47
6.1	Steady state analysis of SRM using FEA	47
6.2	Transient Analysis of SRM using FEA	48
6.3	Results discussion	49
A	Magnetic Material Data Sheet	52

Bibliography

53

List of Figures

1.1	Magnetic Co-Energy plot for the Bar magnet system[1]	2
1.2	Rotor Bar magnet system analysis in the aligned position	3
1.3	Magnetic Co-energy evaluated with the rotor at the 45° tilt position	4
1.4	Inductance Profile of the bar magnet system with Trapezoidal approximation[2]	6
1.5	Dynamic model of the SRM[3]	7
2.1	Inductance variation with the rotation angle	11
2.2	Asymmetric converter to drive the 3-phase SRM[4]	12
2.3	Current variation with the change of the inductance profile[5]	13
2.4	Current waveforms at different speeds of the SRM[5]	14
2.5	Energy Conversion loop in the low speed motoring region[3]	15
2.6	Fluxing and defluxing intervals of SRM[3]	16
2.7	Comparison of the energy conversion loops at different speeds[3]	17
2.8	Control Strategies for SRM at different speed levels[5]	18
3.1	BH curve of the Magnetic Material M300-35A from the datasheet	21
3.2	Interpolated BH curve of M300-35A	21
4.1	Approximation of the SRM Co-Energy plot[4]	24
4.2	Desired Torque Speed Characteristics of the SRM	25
4.3	Plot for the evaluation of the inductance in the region-1[6]	30
4.4	Plot for the evaluation of the inductance in the region-2[6]	31
4.5	Plot for the evaluation of the inductance in the region-3[6]	32
4.6	Variation of flux path lengths with the radial angle[6]	33
4.7	Initial SRM Sizing Algorithm Flowchart	34
4.8	Effect of the change in excitation current on the operating point[5]	34
5.1	Actual geometry for the Rotor pole height calculation	38
5.2	Geometry plots	39
5.3	Stator and Rotor pole enclosures for area calculation	40
5.4	Reluctance network for the calculation of the slot current density[4]	41
5.5	Stator slot current density feasible values	41
5.6	Geometry plots after eliminating infeasible D values	42
5.7	Plot of the Aligned flux linkage vs the bore diameter	43
5.8	Aligned inductances variation with excitation	44
5.9	Area of the Co-Energy Loop calculated	44
5.10	Unaligned inductance and aligned saturated inductance variation with the current	45
5.11	Flowchart of the Magnetic Co-Energy Sizing Algorithm	45

5.12	Variation of Saliency Ratio with the excitation current	46
6.1	FEA analysis of 6/4 SRM in the aligned position	48
6.2	FEA analysis of 6/4 SRM in the unaligned position	48
6.3	FEM aligned transient analysis with an excitation of 10 A	49
6.4	FEM aligned transient analysis with an excitation of 500A	49
6.5	FEM aligned transient analysis with an excitation of 1250 A	50
6.6	FEM aligned transient analysis with an excitation of 2950A	50
6.7	Plot of Stator tooth flux density in a transient analysis	51
6.8	Comparison of Flux linkage plot calculated by Analytical and FEM methods .	51

List of Tables

- 3.1 Magnetic properties of Materials 19
- 3.2 Typical Magnetic properties at 50Hz 19
- 4.1 Geometric design of the Switched Reluctance Machine 29

Abbreviations

L_{au} Aligned **u**nsaturated **I**nductance

L_{as} Aligned **s**aturated **I**nductance

L_u **U**naligned **I**nductance

ϕ_{as} Aligned **s**aturated **F**lux

λ_{as} Aligned **s**aturated **F**lux linkage

Physical Constants

$$\text{permeability of air } \mu = 4 \pi \times 10^{-7}$$

Symbols

B_{sp}	Stator tooth flux density	Tesla
A_{sp}	Specific electrical loading	AT/m
D_o	Outer Diameter	mm
D	Bore Diameter	mm
D_{sh}	Shaft Diameter	mm
w_{sp}	Stator pole width	mm
w_{rp}	Rotor pole width	mm
b_{sy}	Stator backiron thickness	mm
b_{ry}	Rotor backiron thickness	mm
L_{st}	Stack length	mm
h_{sp}	Stator pole height	mm
h_{rp}	Rotor pole height	mm
A_{st}	Area of the stator tooth	mm ²
A_{rt}	Area of the rotor tooth	mm ²
A_{sy}	Area of the stator yoke	mm ²
A_{ry}	Area of the rotor yoke	mm ²
l_{st}	length of the flux path in the stator tooth	mm
l_{rt}	length of the flux path in the rotor tooth	mm
l_{sy}	length of the flux path in the stator yoke	mm
l_{ry}	length of the flux path in the rotor yoke	mm
τ_{sp}	Stator pole pitch	rads
τ_{rp}	Rotor pole pitch	rads
β_{sp}	Stator pole arc	rads

β_{rp} Rotor pole arc rads

For/Dedicated to/To my...

Chapter 1

Introduction to Switched Reluctance Machines

Switched Reluctance Machines are a subject of renewed interest considering the potential that they have to substitute Permanent Magnet synchronous motor drives for automotive applications. The thrust of this thesis work will be to analyze an SRM Motor drive analytically in detail such that it conforms to the performance characteristics desired. The analytical design will be backed up and validated by finite element numerical solutions.

In this chapter a brief introduction is provided for SRM machines highlighting their differences from conventional AC machines. The principle of operation is discussed which is important to comprehend before embarking on with the detailed design process. The dynamic model of the SRM machines will be presented and a simplified bar-electromagnetic rotor model will be solved. The performance metrics evaluated from the simple bar magnet will aid in the design of the actual machine topology later on by explaining the design process. The chapter will conclude by enlisting some major advantages and peculiarities of SRM drives over other AC machine counterparts

1.1 Principle of Operation

Consider a rotor bar electromagnet system where the coil is wound on the bar and is excited with a dc current. The current sets up a flux in the bar which passes through the airgap, links with the rotor and completes the path. The system is an electromagnetic system where the input ports are electrical and the rotor is capable of mechanical rotation. Thus there is an

electromechanical energy conversion that has to take place in order for the system to work.

$$dW_{elec} = dW_{fld} + dW_{mech} \quad (1.1)$$

The input change in electrical energy is equivalent to the change in the field energy and the change in mechanical output energy considering an ideal lossless system. Considering the flux linkage vs current plot in Fig.1.1 as the rotor moves from position x_1 to position x_2 , the linkage flux undergoes a change from λ_1 to λ_2 .

$$dW_{elec} = \int_{\lambda_1}^{\lambda_2} i d\lambda = i(\lambda_2 - \lambda_1) = \text{Area } abcd$$

The change in the stored field energy will be equal to the difference between the field energies

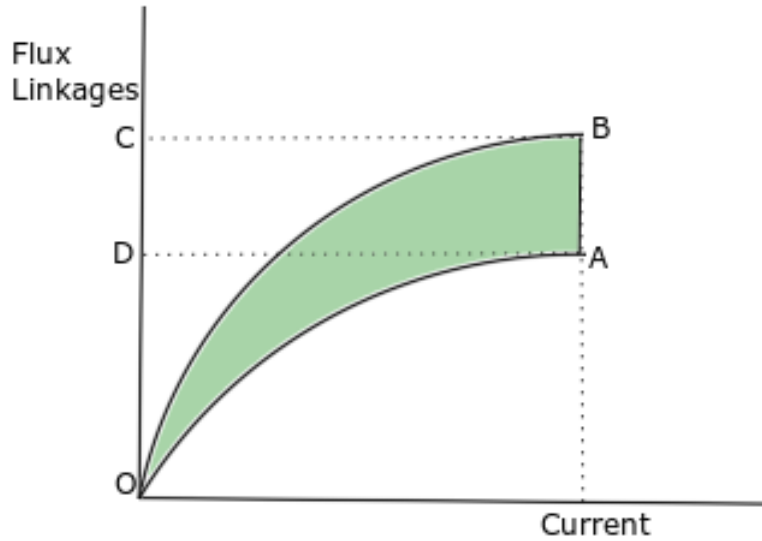


FIGURE 1.1: Magnetic Co-Energy plot for the Bar magnet system[1]

at position x_2 and x_1 respectively.

$$dW_{fld} = \text{Area}(obc) - \text{Area}(oad)$$

From (1.2) the change in mechanical energy can be written as

$$dW_{mech} = \text{Area}(abcd) - (\text{Area}(obc) - \text{Area}(oad)) = \text{Area}(oab)$$

Area(oab) is equal to the change in the magnetic co-energy and thus the output mechanical energy can be expressed as

$$dW_{mech} = dW_{fld}$$

$$T_m = \frac{\partial W_{fld'}}{\partial \theta} \Big|_{i=const} \quad (1.2)$$

The output developed electromagnetic torque can thus be expressed as the ratio of the change in the magnetic co-energy wrt the angular rotation keeping the excitation constant.

1.1.1 Torque Calculation using the Co-Energy method

For the simplified rotor bar electromagnet system the torque can be calculated by applying the principles developed in the previous section. Fig.1.2 shows the system with the rotor in the aligned position. Using FEA simulation the field energy in the aligned position is

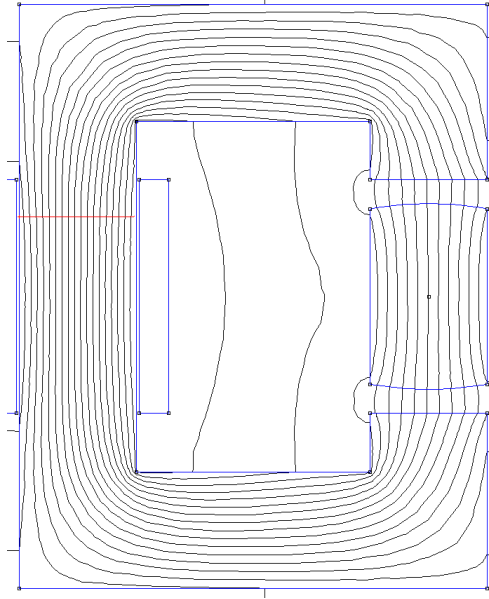


FIGURE 1.2: Rotor Bar magnet system analysis in the aligned position

calculated as

$$W'_{fld_{0^\circ}} = 0.005327J$$

Similarly running another FEA simulation this time with the rotor at a 45° tilt position from the centre

$$W'_{fld_{45^\circ}} = 0.004239J$$

$$\Delta W'_{fld} = W'_{fld_{0^\circ}} - W'_{fld_{45^\circ}} = 0.00111J$$

$$\Delta\theta = \pi/4 \text{ rads}$$

$$T = \frac{\Delta W'_{fld}}{\Delta\theta} = 0.0015Nm$$

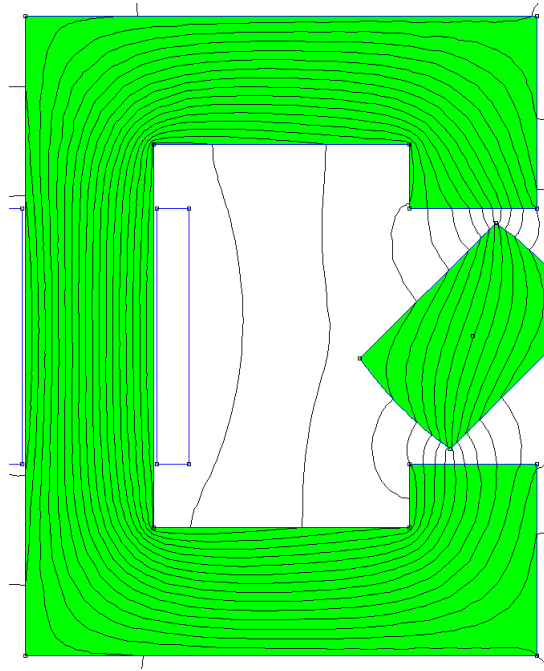


FIGURE 1.3: Magnetic Co-energy evaluated with the rotor at the 45° tilt position

1.1.2 Torque analysis using Inductance Variation

The system described can also be solved in terms of the inductances. The system is assumed as magnetically linear as well as with a constant excitation. Thus the rate of change of field energy can be expressed as the familiar expression.

$$\Delta W_{fld} = d/dt\left(\frac{Li^2}{2}\right) \quad (1.3)$$

which results in the following useful expressions

$$P_{mech} = \frac{i^2}{2} dL/dt$$

$$T_{mech} = \frac{i^2}{2} dL/d\theta \quad (1.4)$$

The system at the 0° position can be analyzed by FEA analysis as well as using analytical calculations to find the inductance in the aligned position since the fringing effects are negligible.

In the given problem 100 turns are wound around the electromagnet and a constant excitation current of 50A is applied.

1. Finite element analysis

The flux passing through the core is calculated using FE simulation. The aligned inductance is evaluated by dividing the flux linkage by the excitation current. Normal

flux : 0.00089Wb

$$\lambda = N\phi = 0.089\text{Wb}$$

$$L_{a_{FEA}} = \frac{N\phi}{i} = 1.618 * 10^{-4}$$

2. Analytical calculation

The inductance in the aligned position can also be calculated by solving the electromagnetic circuit corresponding to the configuration in Fig.1.2. The magnetomotive force along the contour can be written as

$$F = Ni = \phi R_t \tag{1.5}$$

The total reluctance for the magnetic circuit shown in Fig.1.2 is equal to the summation of the reluctances of all the magnetic paths.

$$R_t = 3R_{p1} + 2R_{p2} + 2R_g + R_r$$

However the total reluctance can be approximated by only the reluctance of the gap as it's permeability is orders of magnitude lower than that of iron.

$$R_g = \frac{2l_g}{A_g\mu_o}$$

The length of the gap and the depth are calculated using FEM which results in the calculation of the total reluctance

$$R_t = 5.3 * 10^6$$

Using (1.5) the flux can now be calculated

$$\phi_a = 0.00096\text{Wb}$$

$$L_{a_{Anal}} = 1.680 * 10^{-4}\text{H}$$

1.1.3 Inductance Profile

For building the inductance profile of the simple rotor bar magnet system as a function of the rotation angle θ it is necessary to evaluate the inductances at different discrete positions of the rotor angle. However to simplify the analysis the trapezoidal approximation is used

where the inductances are evaluated at the extremal positions of 0° and 90° . FEA analysis is used to calculate these inductances.

1. Rotor at 0° position

$$L_{0^\circ} = 0.0017H$$

2. Rotor at 90° position

$$L_{90^\circ} = 0.00124H$$

For the torque calculation inductance variation wrt the change in position can be found out as

$$dL/d\theta = \frac{L_{max} - L_{min}}{\pi/2}$$

$$T_{avg} = \frac{i^2}{2}dL/d\theta = 0.72Nm$$

The torque is motoring or generating depends upon the derivative of the inductance profile. If the motoring torque is desired only the positive slope part is considered. For the trapezoidal approximation of the inductance profile shown in Fig.1.4 the mean motoring torque can be calculated as

$$MMT = \frac{(\pi - \pi/2)T_{avg}}{\pi} = 0.36Nm \quad (1.6)$$

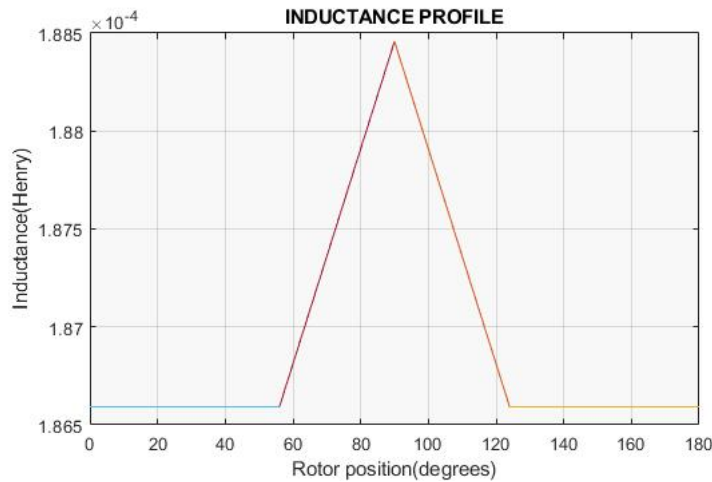


FIGURE 1.4: Inductance Profile of the bar magnet system with Trapezoidal approximation[2]

1.1.4 Dynamic Model of SRM

For the performance analysis of switched reluctance machines and instantaneous torque calculation recourse has to be taken to the dynamic model as shown in Fig.1.5. The model

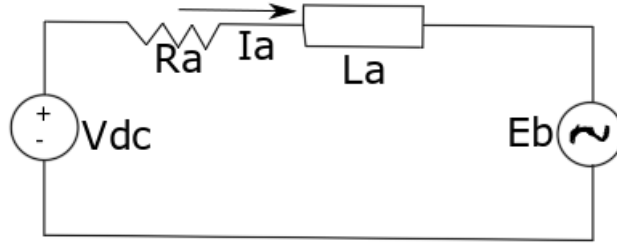


FIGURE 1.5: Dynamic model of the SRM[3]

differs from conventional AC machines in that the flux changes are dependent both on the excitation current as well as the rotation angle.

$$\begin{aligned}
 V &= Ri + p\psi(i, \theta) \\
 V &= Ri + \frac{\partial \lambda(i, \theta)}{\partial i} \frac{di}{dt} + \frac{\partial \lambda(i, \theta)}{\partial \theta} \frac{d\theta}{dt} \\
 V &= Ri + L \frac{di}{dt} + k_b \omega_m
 \end{aligned} \tag{1.7}$$

The last term of equ(1.7) is the back emf term

$$E_b = k_b \omega_m$$

The torque developed can be written as

$$\tau_d = \frac{E_b i_a}{\omega_m}$$

For the bar magnet system under consideration the instantaneous torque developed at the 45° position with a fixed dc current of 50A

$$\tau_d = \left(\frac{\lambda^0 - \lambda^{45}}{\pi/4} \right) * 50$$

$$\tau_d = 0.445 Nm$$

1.2 Advantages of Switched Reluctance Machines

SRM machines are also known as doubly salient reluctance machines. Both the stator as well as the rotor are salient in nature. DC pulses are fed to pole windings with power switches. Flux created by the DC current tends to turn the rotor in a direction so as to minimize the reluctance. When a certain phase experiences minimum reluctance in its path, another phase is excited which at that moment experiences a higher reluctance. That phase then in turn tries to reach a position of minimum reluctance. The switching of currents thus causes the change in reluctance

- When rotor poles are aligned stator phase current is turned off and another stator winding excited. Thus at a certain instant only one phase is excited requiring only one power switch making the drive economical.
- The SRM drive provides a good starting torque as it is similar to a dc series motor providing a torque which is proportional to the square of the current.
- The SRM drive is particularly suitable for regenerative action as by only changing the polarity of the current it is possible to develop a generating torque. This is in contrast to Induction machines where a bidirectional converter is needed for regenerative braking.
- The SRM drives are inherently dependent on a power electronics converter to implement the control action. This makes them good candidates for variable speed operation.
- For SRM drives the motoring torque is produced for a short duration in pulsed form as the operation is limited to the positive derivative of the inductance profile.
- SRM machines have a simple and robust structure. The rotor does not carry permanent magnets like PMSM drives. Neither does it have bars like Induction machine drives. Fast torque dynamics comparable to PMSM drives have brought them into the limelight of research for automotive applications.
- With the difficulties in procurement of rare-earth magnets like Neodymium and Dysprosium there has been an emphasis on research for rare earth free and ferrite magnet assisted machines. Coupled with suitable control strategies SRMs can provide a fairly wide constant power speed region which is desirable for automotive applications.

Chapter 2

Background Review of Switched Reluctance Machines

The design of SRM drives are dependent upon the topology of the machine which is selected. The topology can be selected based on the target application area and a host of other factors. Since the inductance profile is dependent on the topology being selected a 6/4 SRM machine is selected and the ensuing design will be proceeded on with that topology. The 3-phase 6/4 SRM drive is suitable for the target area of automotives which lie in the small-medium power range.

In this chapter at first the inductance profile will be developed for our selected 6/4 SRM machine. The relationship between the flux and the current as a function of the angle will be examined in detail.

A comparison of the control strategies of conventional AC machines will be done and then the different modes of operation of SRM drives will be examined. The control strategies for the different modes of operation will be discussed briefly and to conclude some common SRM drive architectures will be presented.

2.1 Inductance profile of the 6/4 SRM machine

The SRM with 6 stator poles and 4 rotor poles is selected for our design. The corresponding pole pitches can be evaluated

$$\tau_{sp} = \frac{360}{6} = 60^\circ \quad (2.1)$$

$$\tau_{sp} = \frac{360}{4} = 90^\circ \quad (2.2)$$

Next the pole enclosure ratios are selected based on design experience. The torque density is good for pole enclosures in the range of 0.3-0.5. To proceed with our design a pole enclosure ratio of 0.4 is chosen for the stator pole while 0.5 is chosen for the rotor pole.

$$k_{sp} = \text{statorpole} : \text{statorpolepitch} = 0.4 \quad (2.3)$$

$$k_{rp} = \text{rotorpole} : \text{rotorpolepitch} = 0.5 \quad (2.4)$$

The pole arcs can be evaluated as follows

$$\beta_s = k_{sp} * \tau_{sp} = 24^\circ$$

$$\beta_r = k_{rp} * \tau_{rp} = 45^\circ$$

The starting point 0° is considered at L_{min} where the end point of the rotor pole coincides with the starting point of the stator pole. As the rotor nows moves the airgap between the projecting stator and rotor poles decreases and thus flux linkages increase.

The inductance rise continues till the point where all of the rotor tooth sees a uniform airgap. After that point the inductance remains unifrom at it's max value L_{max} . When the rotor nows moves further the flux linkages start to decrease and hence the inductance starts its descent towards it's minimum value. The inductance stays at the minimum value till the rotor comes underneath a different phase which is excited and the cycle continues.

Fig.2.1 shows the derivative of the inductance profile which is positive for the rising part of the inductance profile while it is negative for a decreasing current profile. Since the derivative appears as a quasi-square wave hence the torque has a pulsating nature. For motoring operation the current is injected in the positive derivative region of the inductance. The current has to rise as well as fall to zero before the negative pulsating region starts because if the current is still present in the negative region it would lead to generating action.

2.1.1 Relationship between the flux and the rotation angle

A simplified model of an SRM excited phase can be represented where a dc voltage is applied across an inductance and a free-wheeling diode is connected in anti-parallel configuration. The terminal relation can be written as follows

$$v = ri + Nd\phi/dt \quad (2.5)$$

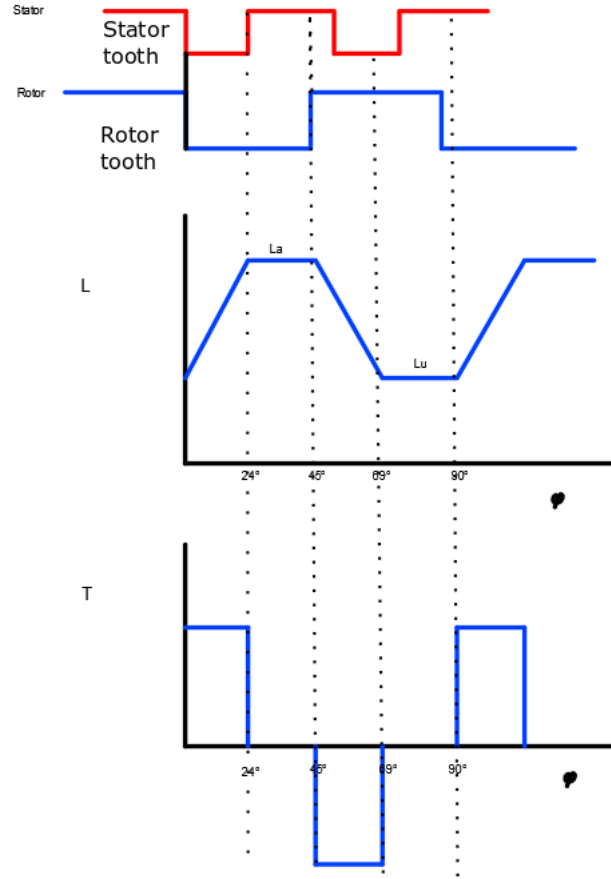


FIGURE 2.1: Inductance variation with the rotation angle

The resistance drop is small compared to the induced emf and hence it can be ignored for analysis.

$$V_{dc} = Nd\phi/dt$$

$$\phi = \int (V_{dc}/N)dt$$

The integration variable can be changed to the angle θ and the following relationship is derived

$$\phi = \int (V_{dc}/N\omega)d\theta \quad (2.6)$$

Given that the applied voltage is a dc and the speed of the machine is constant the flux increases directly with the angle of rotation. The flux increases in the positive direction during the rising slope of the inductance because a positive voltage is applied across the windings. Before the inductance profile starts to go in the decreasing trend the polarity of the applied voltage is reversed and according to equ(2.6) the flux now starts to decrease with increasing angle.

Thus the reversal of polarity is required of the applied voltage and hence a unique type of converter is required for such an action to take place. A commonly used system is the double

supply switch-diode converter configuration shown in Fig.2.2. When the switch is ON the

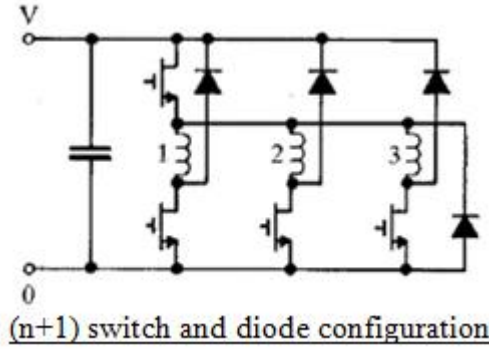


FIGURE 2.2: Asymmetric converter to drive the 3-phase SRM[4]

voltage v_{ab} is positive with the polarity shown. When the switch is turned OFF freewheeling action takes place through the diode and v_{ab} attains a negative polarity.

Fig.2.1 shows that the speed response of an SRM drive is quite fast as it directly varies with $dL/d\theta$. Rotor inertia of the drive is small thereby enabling fast torque dynamics

2.1.2 Relationship between the flux and the current

Flux increases with the current when V_{dc} is applied across the windings. Therefore the inductance can be written as a function of the flux as follows

$$L = N\phi/i \tag{2.7}$$

Substituting the relation for the flux from equ(2.6) into (2.7) we get

$$i = \frac{V_{dc}\theta}{\omega L} \tag{2.8}$$

Thus the current that establishes across the winding is a function both of the inductance as well as that of the speed of the machine.

When the inductance is at its minimum value of L_{min} the rise of the current is steep if constant speed is considered according to the following relation

$$di/dt = V_{dc}/L_{min}$$

When the inductance profile starts to increase however according to Fig.2.3 the rise of the current gets arrested because the inductance resists the change in current. Also the same effect can be noted during the decaying current waveform that decay is slow when the inductance

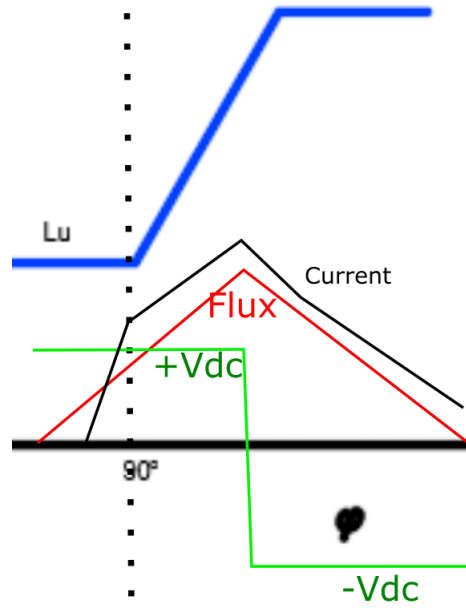


FIGURE 2.3: Current variation with the change of the inductance profile[5]

is at its maximum value L_{max} . Further it can be noticed that the negative polarity of the voltage is applied quite early so as to allow sufficient time for the current profile to decay to zero. If the negative pulse is applied with delay the current may still exist during the generating region of the torque profile.

2.2 Modes of Operation of the Switched Reluctance Machine

Whenever the inductance of the SRM is changing the $dL/d\theta$ term in the torque expression would appear as a constant. Hence the torque expression can be written as

$$T = 1/2 \frac{i^2 dL}{d\theta} = ki^2 \quad (2.9)$$

Substituting the expression of the current from equ(2.6) into equ(2.9) we get the following

$$T = k \frac{V_{dc}\theta}{\omega L} \frac{V_{dc}\theta}{\omega L} \quad (2.10)$$

$$P_{out} = T\omega = \frac{kV_{dc}^2\theta^2}{\omega L^2}$$

If the speed is very low the current value will be higher and chop mode control for the current would be used for maintaining the current at its reference value. At somewhat higher speeds

the current decreases to a smaller value and a different control strategy is employed. At this higher levels of speed than the base speed the current value further shrinks. The current vs the rotation angle plot for the different modes of operation of the SRM drive are surmised in Fig.2.4

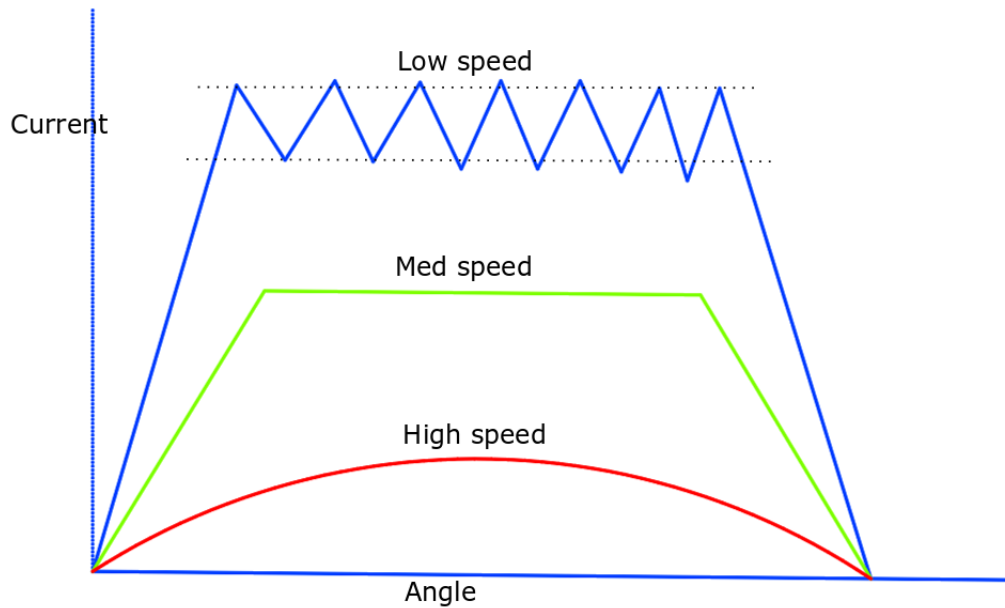


FIGURE 2.4: Current waveforms at different speeds of the SRM[5]

2.3 Control Strategy for SRM drives

At low speeds the torque is limited primarily by the current. PWM voltage or current regulation is the primary mode of control. At high speeds the back emf increases and there is insufficient voltage available to regulate the current. At high speeds the timing of the current pulses are changed to achieve the control action known as Advanced angle control.

To contrast with control of conventional AC machines there is no equivalent of Field-Oriented control(FOC) for SRM machines. The torque is produced in impulses. The flux has to be built from zero and has to return to zero in each stroke of the machine. The orthogonality of the flux and the current as that in dc machines or that employed for control in FOC of AC machines is not present in SRM machines.

In induction the windings are distributed sinusoidally and the airgap is smooth. In such case space vectors can be used to resolve the mmf distribution.

2.3.1 SRM Low speed operation

At the instant of starting of the machine the back-emf e is low as the speed is low

$$e = \partial\phi/\partial t = \omega_m \partial\phi/\partial\theta \quad (2.11)$$

As the speed is low the term $V_s - e$ or $-V_s - e$ is available to raise or lower the flux level. According to Fig.2.4 the current is being regulated at a reference value according to chop-mode control. At the start at point(1) as the inductance is constant and the current is increased the flux level increases. When the current reaches its maximum value @point(2) the torque starts to rise.

When the current is kept at its maximum value and the inductance starts to increase with the rotation angle the flux starts rising known as the fluxing region. This behavior continues till point(A). After that point the flux starts to drop as the current is reduced to zero known as the defluxing region.

At low speed operation the operation can be represented by the energy conversion loop as in Fig.2.5. The point U corresponds to the point in the unaligned position between the stator

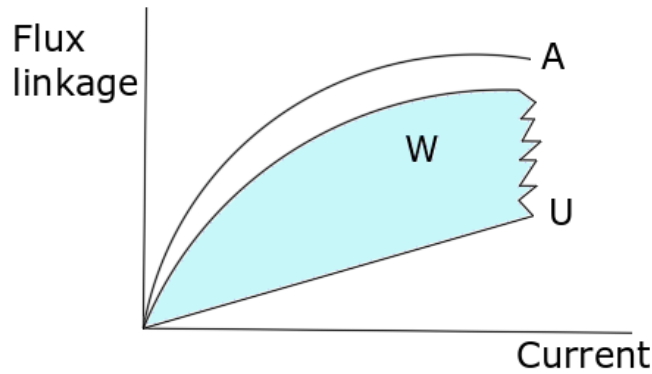


FIGURE 2.5: Energy Conversion loop in the low speed motoring region[3]

and rotor axes. The area of the energy conversion loop can be extended by retarding the commutation angle.

2.3.2 High speed motoring operation

At high speeds the governing relation for the rise of current can be expressed as

$$V_s - e = di/dt \quad (2.12)$$

Thus when the speed approaches the base speed ω_b the switches must remain as chopping would reduce the avg voltage and the voltage won't be enough for the current to rise. According to equ(2.11) the change in flux level can be expressed as

$$d\phi = \Delta\theta V_s / \omega \quad (2.13)$$

Thus to maintain the peak flux at the same level the dwell should be increased linearly with speed. However the dwell can only increase till the time where the fluxing and the defluxing intervals are equal and their sum is equal to the rotor pole pitch conduction stroke of 90° . Fig.2.6 shows the instant where the fluxing and the defluxing intervals become equal and the dwell may not be further increased.

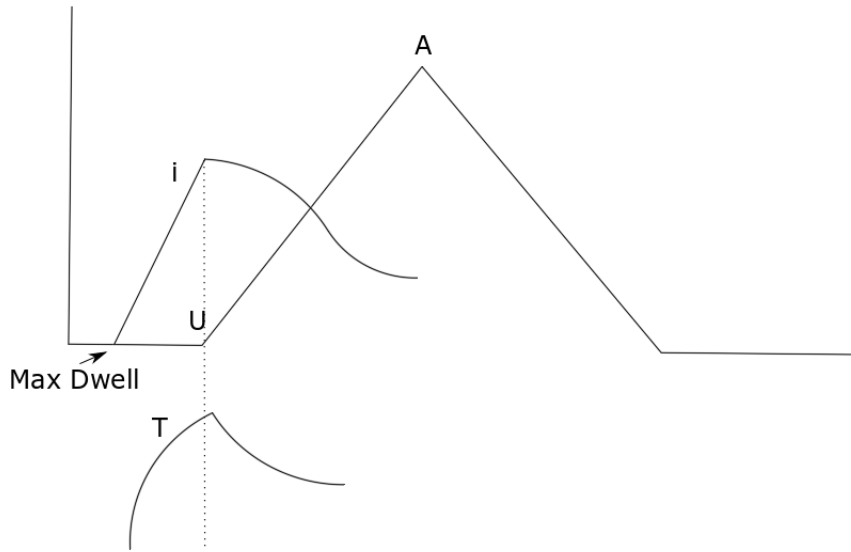


FIGURE 2.6: Fluxing and defluxing intervals of SRM[3]

The constant power region is thus not possible over a wide range of operation due to the limitations of the maximum dwell. If the speed increases three times and dwell increases from its start point of 30° to 45° then the peak flux must change according to the equ(2.13)

$$d\phi = 1.5 * V_s / 3 = 0.5$$

Fig.2.7 shows the energy conversion loops at both the speeds of ω and 3ω . The corresponding peak of the energy conversion loop has halved as can be seen and also the area of the energy conversion loop has also decreased which corresponds to the torque that can be extracted from the machine.

The constant power can be maintained if the loss in the area of the energy conversion loop can be compensated by a corresponding increase in speed.

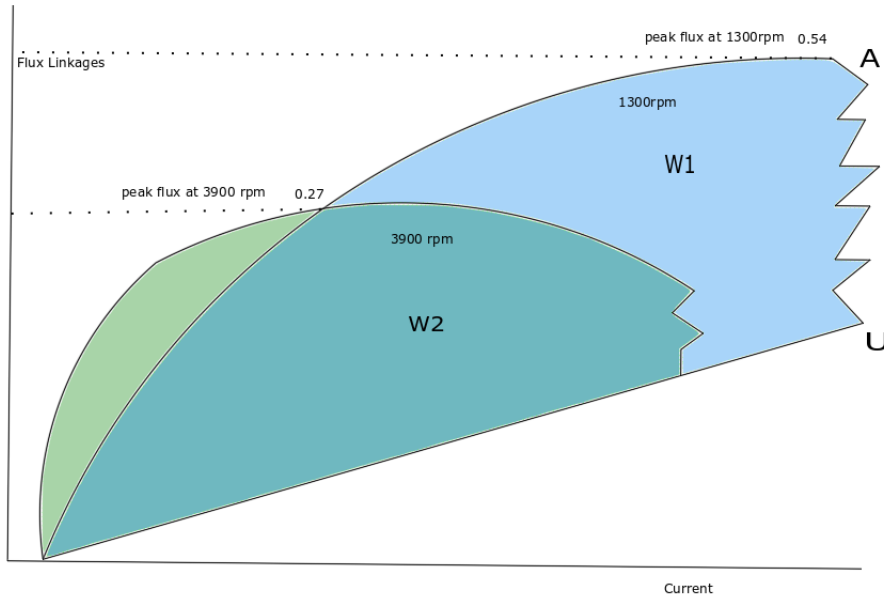


FIGURE 2.7: Comparison of the energy conversion loops at different speeds[3]

$$P = T\omega = W\omega$$

$$\Delta P = \Delta W\omega + \Delta\omega W = 0$$

$$\Delta W/\omega = -\omega/\Delta\omega \quad (2.14)$$

If the relation given by equ(2.14) is not fulfilled then the machine leaves the constant power operating region and enters the $T\omega^2 = \text{constant}$ operating region.

2.3.3 Control strategies for the different modes of operation

Fig.2.8 shows the different modes of operation of the SRM drive depicted as torque against the speed plot. The control strategies for these different modes of operation are presented briefly.

1. Chop mode Control

At low to mid speed operation the current i is maintained within two bands by switching the input voltage between V_{dc} and $-V_{dc}$. Also known as the torque control mode the torque is controlled by keeping the current constant.

2. Advanced Angle Control

The current is not kept constant here but rather the product of the torque and the

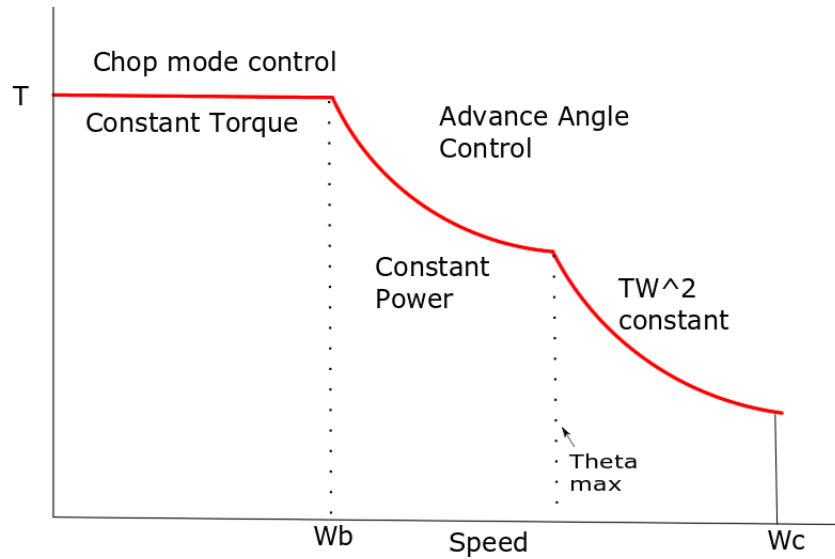


FIGURE 2.8: Control Strategies for SRM at different speed levels[5]

speed is kept constant by retarding the commutation angle also known as the advance angle.

$$P = T\omega = \frac{kV_{dc}\theta_o}{\omega L} \frac{kV_{dc}\theta_o}{L} = const$$

Where θ_o is known as the advance angle and it is changed with the change in speed.

3. $T\omega^2$ control

When θ_o reaches its maximum angle the dwell can no longer be further extended and hence the machine enters $T\omega^2$ control region

$$T\omega^2 = kV_{dc}^2\theta_o^2/L^2 = const$$

Chapter 3

Magnetic Material

Selection of the material for the machine design is of paramount importance. The material must exhibit low hysteresis loss and high magnetic polarization properties. Non oriented steels provided by the Cogent Power ltd are used for the design of the core which are graded according to European standards EN 1016. The datasheet is attached in Appendix A. Table

Grade(EN10106)	Thickness(mm)	Max Specific loss(mW/kg)1.5T	$H_{min} = 5000(AT/m)$	$H_{min} = 10,000(AT/m)$
M235-35A	0.35	2.35	1.60	1.70
M250-35A	0.35	2.50	1.60	1.70
M300-35A	0.35	3.00	1.60	1.70

TABLE 3.1: Magnetic properties of Materials

3.1 shows the magnetic properties of the materials shortlisted for the design at hand. 35mm is chosen as the thickness of the material as a thinner material is required to minimize the eddy current losses. The minimum magnetic polarities of the materials are the same at the applied magnetic field intensities of 5000 AT/m and 10,000 AT/m. The specific loss however is the lowest for the material M235-35A. For medium sized machines higher permeability

Grade(EN10106)	Max Specific loss(mW/kg)1.5T	$H_{min} = 5000(AT/m)$	$H_{min} = 10,000(AT/m)$	permeability μ_r
M235-35A	2.35	1.64	1.76	610
M250-35A	2.50	1.64	1.76	660
M300-35A	3.00	1.65	1.78	830

TABLE 3.2: Typical Magnetic properties at 50Hz

is preferred whereas power loss is a more important governing concern for large machines.

Usually concentration of an alloy such as Silicon is embedded in the material which helps in reducing the losses however reduces the permeability of the material. For our design material will low carbon alloy content with higher losses but higher permeability and low cost is chosen.

3.1 Salient points about the Material Selection

1. Thickness chosen on the lower side[0.35mm] to reduce eddy current losses. Max specific loss for M300-35A on the higher side for peak flux densities of 1.0T and 1.1T. Those for M235-35A and M250-35A are comparable.
2. Magnetic polarization for M300-35A on the higher side. For the magnetic field strengths of 2500,5000 and 10000 AT/m permeability of M300-35A quite better than M235-35A and M250-35A.
3. Mechanical properties of M235-35A are superior. higher resistivity and better tensile strength than the other two.
4. HP grades although have a higher specific loss and thickness. Their minimum magnetic polarization is quite high compared to cogent grades. For example the HP grade material M530-50 HP has a minimum magnetic polarization of 1.81T @ 1000 A/m field intensity. M235-35A however has a minimum B of 1.70T @ 1000 A/m. Alloy content reduces losses but also decreases the permeability at high field strengths so materials with low silicon contents are selected.

In light of the above discussion the material M300-35A is chosen for the ensuing design of the SRM drive.

3.2 Magnetization curves of M300-35A

Fig.3.1 shows the BH magnetization curve of the magnetic material M300-35A chosen for our design problem. The manufacturer typically provide some points in the linear region and as well in the saturation. However for accurate characterization of the magnetization properties the BH curve is imported from MAGNET software as shown in fig.3.2.

The BH points from MAGNET are interpolated using spline interpolation and the flux densities and field intensities are assumed for the remaining analysis. A peak flux density of 1.9T from the BH curve is selected for the stator tooth which experiences the highest level of saturation. For the knee point a flux density of 1.6T Tesla is selected.

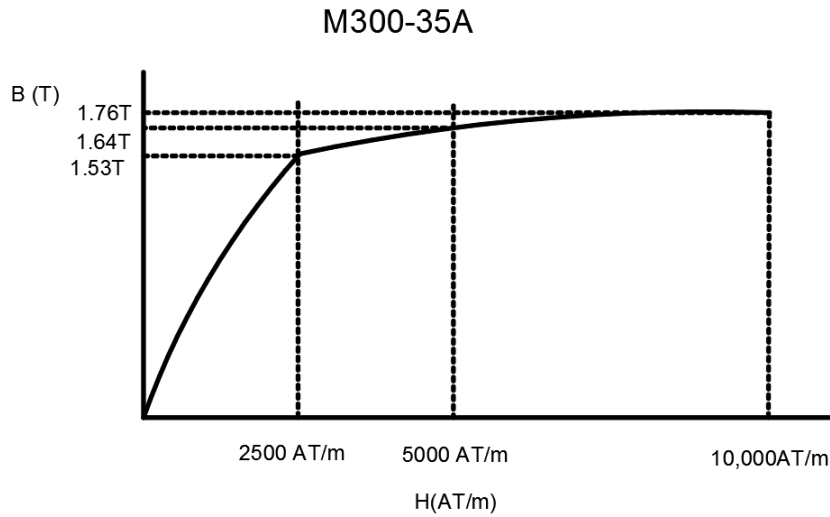


FIGURE 3.1: BH curve of the Magnetic Material M300-35A from the datasheet

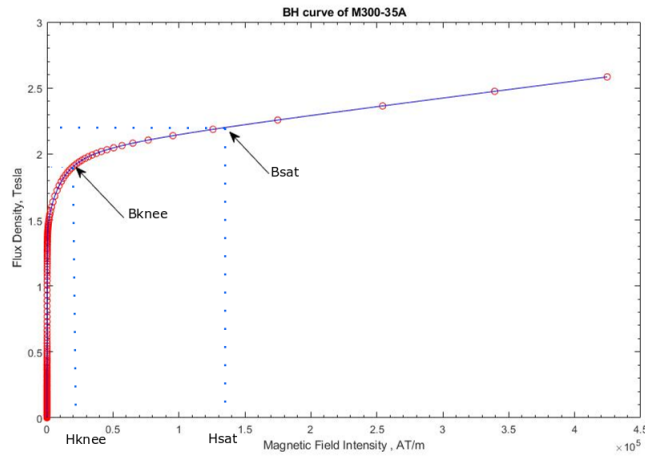


FIGURE 3.2: Interpolated BH curve of M300-35A

3.2.1 Estimation of SRM design Ratios

Know that the stator saturated tooth flux density and the knee point flux density is known some important design ratios can be calculated

$$\lambda_{as} = N\phi_{as} = L_a^s * i_{pk} = B_{st} * A_{sp}$$

$$\lambda_{au} = N\phi_{au} = L_a^u * i_{kn} = B_{kn} * A_{sp}$$

$$\sigma_\lambda = \frac{\lambda_a^u}{\lambda_a^s} = \frac{B_{kn}}{B_{st}} \quad (3.1)$$

$$\frac{H_{kn}}{H_{st}} = \frac{Ni_{kn}}{Ni_{pk}}$$
$$\sigma_i = \frac{i_{kn}}{i_{pk}} \quad (3.2)$$

The flux linkage saturation ratio σ_λ and the the current saturation ratio σ_i are evaluated from the BH curve of the material. These ratios will come handy during the designing with the torque sizing equation.

Chapter 4

Initial Sizing of the SRM drive

4.1 Key considerations for the design of SRM drives

The performance of SRM drives depend on the following

1. Dimensions of Stator and Rotor laminations
2. Winding details
3. Pole number
4. Pole arc lengths

The output power equation is the approximate starting point for the initial sizing of SRM machines and then the design is iterated to meet steady state performance requirements. The output equation of the SRM is a relation that links the machine's volume, speed and electric, and magnetic loadings to the output of the machine.

Fig.4.1 shows the typical flux linkage vs excitation current plot for the SRM. The actual trajectory of the aligned inductance is curvilinear in nature however it is approximated by segmenting it into separate regions i.e. the aligned unsaturated inductance L_a^u uptill the knee point current and the aligned saturated inductance L_a^s after that point. The area enclosed within the aligned and the unaligned inductance inductance boundaries represents the output mechanical energy per stroke that can be extracted from the machine.

The applied voltage across the stator pole windings can be expressed as

$$V = d\lambda/dt = \frac{\lambda_a - \lambda_u}{\lambda_u} \quad (4.1)$$

The inductances are expressed in terms of the leakage factors defined as follows

$$\sigma_s = \frac{L_a^s}{L_u}$$

$$\sigma_u = \frac{L_a^u}{L_u}$$

The SRM performance depends on its operating point k_o which is defined as the following expression

$$k_o = 1 - \frac{1}{\sigma_u \sigma_s} \quad (4.2)$$

Flux-Linkage vs Current Plot

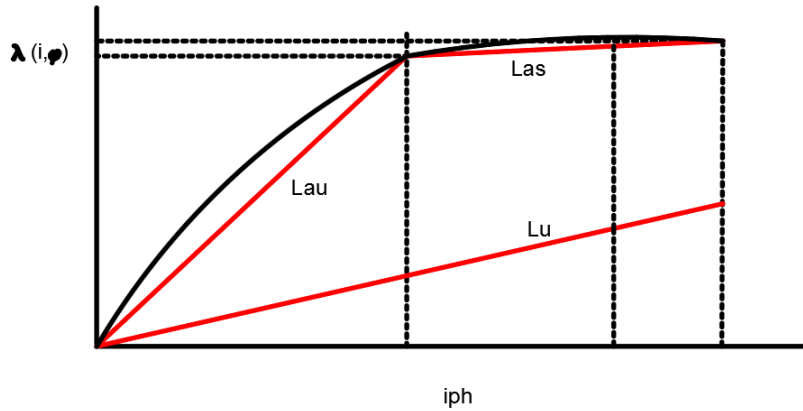


FIGURE 4.1: Approximation of the SRM Co-Energy plot[4]

4.2 Design Specifications

The design specifications of AC machines are usually given in terms of the torque versus speed and the Power versus speed curves. The designed machine is expected to provide a constant output torque till the base speed and then from the base speed up till the maximum speed the machine goes into the constant power mode. The maximum operating speed of the machine is determined by its speed ratio X .

The Switched Reluctance Machine under consideration is required to meet the following Torque-speed characteristics. From the characteristics it is evident that the machine is required to give a constant output torque of 100Nm till the base speed of 6,200rpm and then

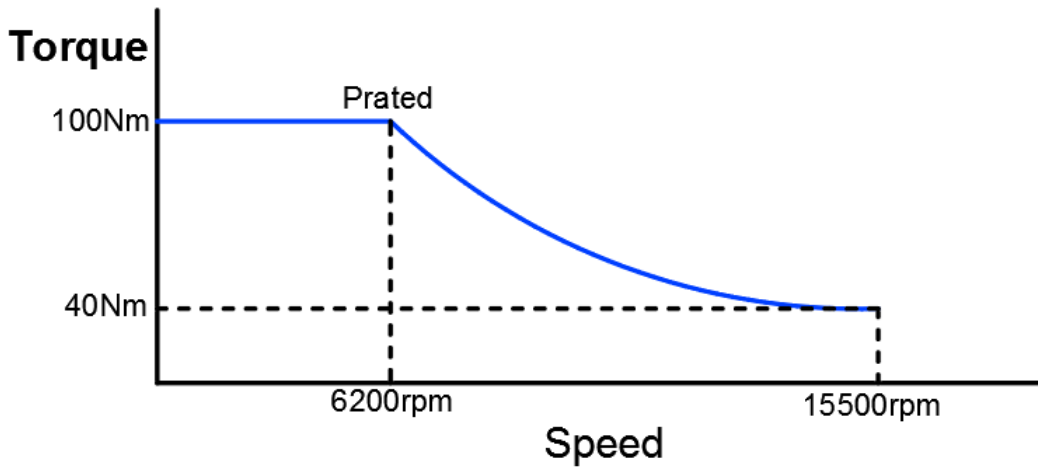


FIGURE 4.2: Desired Torque Speed Characteristics of the SRM

a constant output power of 50kW till the maximum speed of 15,500rpm. The speed ratio X comes out to be 2.5.

Initial Constraints These correspond to the constraints imposed by the manufacturer.

The design requires a power output of 50kW at the base speed with a torque of 100Nm and then it enters into constant power mode with a torque of 40Nm at the maximum speed. The inverter is supplied with the dc voltage of 300V and the outer diameter constraints are of 150mm. The current density is assumed at $10A/mm^2$ and can vary within the range of 4 to $20A/mm^2$. Rated Output Power :- $P_{rat} = 50kW$ Rated Output Torque :- $\tau_{rat} = 100Nm$ base speed :- $\omega_{rat} = 6,200rpm$ maximum speed :- $\omega_{max} = 15,500rpm$ DC link Voltage :- $V_d = 300V$ Stator Outer Diameter :- $D_o = 150mm$ No of Stator poles :- ($P_s = 6, \tau_{sp} = 60^\circ$) No of Rotor poles :- ($P_r = 4, \tau_{rp} = 90^\circ$) Airgap length :- $l_g = 1mm$ Current density :- $J = 10A/mm^2$ Fill Factor :- $k_f = 0.6$

Design Parameters and Proportionality constants

The saturated flux density had already been assumed during the Material selection. Aspect ratio is selected as 0.7. The electrical loading can vary between a dynamic range of 25000 to 90000 At/m. Based on design experience a value of 50,000 At/m is selected.

The pole enclosure ratios play an important role in the torque calculations of an SRM. Again based on design experience values of 0.4 and 0.5 are chosen for the stator and the rotor pole enclosure ratios respectively. The flux splits across the surface of the back iron and that's why the thickness is assumed almost half of that the tooth width so that the same flux density can be maintained.

1. Stator tooth flux density :- $B_{sp} = 1.9T$
2. Aspect Ratio :- $k_{asp} = D/L = 0.7$
3. Specific electrical loading :- $A_{sp} = 50,000At/m$
4. Duty cycle :- $k_d = 1$
5. Operating point :- $k_o = 0.75$
6. Stator tooth to tooth pitch ratio :- ($k_{stp} = 0.4, \beta_s = 24^\circ$)
7. Rotor tooth to tooth pitch ratio :- ($k_{rtp} = 0.5, \beta_r = 45^\circ$)
8. Ratio of Stator yoke height to the Stator pole width :- $k_{sy} = b_{sy}/w_{sp} = 0.6$
9. Ratio of Rotor yoke height to the Stator pole width :- $k_{ry} = b_{ry}/w_{sp} = 0.6$

Design variables

The design variables correspond to the electromagnetic design of the geometry that has to be evaluated and thus constitutes the bucket list.

1. No of turns per phase :- T_{ph}
2. Rotor Bore Diameter :- D
3. Width of the stator pole :- w_{sp}
4. Width of the rotor pole :- w_{rp}
5. height of the stator pole :- h_{sp}
6. height of the rotor pole :- h_{rp}
7. Stator yoke height :- b_{sy}
8. Rotor yoke height :- b_{ry}
9. Shaft Diameter :- D_{sh}

4.3 Calculation of the Bore Diameter

The developed Torque as a function of the design variables is given as

$$\tau_d = k_e * k_d * k_o * \pi/4 * B * A_s * D^2 * L \quad (4.3)$$

Replacing the stack length in terms of the bore diameter using the aspect ratio and putting the values

$$100 = 1 * 0.75 * \pi/4 * 1.7 * 50000 * D^3/0.7$$

$$D = 112mm$$

4.3.1 Stator pole width

The Stator pole width can be expressed in terms of the bore diameter and the stator pole arc as given in equ.2.

$$w_{sp} = D * \sin(\beta_s/2) \quad (4.4)$$

$$w_{sp} = 0.112 * \sin(24^\circ/2) = 23mm$$

4.3.2 Rotor pole width

The Rotor pole width can be expressed in terms of the bore diameter and the stator pole arc as given in equ.2.

$$w_{rp} = D * \sin(\beta_r/2) \quad (4.5)$$

$$w_{rp} = 0.112 * \sin(24^\circ/2) = 34mm$$

4.3.3 Stator yoke height

The Stator yoke height is usually equal to half of the stator pole width as the magnetic flux passing through the back iron splits into half.

$$b_{sy} = 0.6 * w_{sp} \quad (4.6)$$

$$b_{sy} = 0.6 * 23 = 14mm$$

4.3.4 Rotor yoke height

Similarly the flux passing through the Rotor pole also splits across the back iron and can be assumed to be of the same value as that of the rotor yoke height.

$$b_{ry} = 0.6 * w_{sp} \quad (4.7)$$

$$b_{ry} = 0.6 * 23 = 14mm$$

4.3.5 Stator Pole height

The Stator pole height can be calculated by subtracting the bore diameter and twice the stator back iron height from the Stator outer diameter

$$D_o = D + 2 * b_{sy} + 2 * h_{sp} \quad (4.8)$$

$$h_{sp} = \frac{150 - 112 - 28}{2} = 5mm$$

The computed machine parameters from the initial sizing can be surmised in Table 4.1.

4.4 Rotor Pole height evaluation

4.4.1 Permeance Method for Inductance Calculation

The saliency ratio L_a/L_u plays an important role in determining the performance of switched reluctance machines. The value of the inductance constant k_o had been assumed for the initial sizing based on experience but for a more comprehensive design k_o has to be evaluated. Calculation of the unaligned stator phase inductance is a way of determining the saliency ratio as the value of L_u remains constant even when the machine is driven into the saturation region.

The evaluation of the unaligned inductance using the permeance method consists of segregating the machine's geometry based on the flux patterns into three regions. The permeance offered to a flux line in an infinitesimal area dA is given by

$$dp_l = \frac{\mu * dA}{l_l} \quad (4.9)$$

Computed SRM design values		
Stator Dimensions	Rotor Dimensions	Electrical Parameters
$D_o = 150mm$	$D = 112mm$	$P_o = 50kW$
$P_s = 6$	$P_r = 4$	$\tau_r = 100Nm$
$w_{sp} = 23mm$	$w_{rp} = 34mm$	$V_d = 300V$
$b_{sy} = 14mm$	$b_{ry} = 14mm$	
$h_{sp} = 5mm$	$h_{rp} = ?$	
$l_g = 1mm$	$D_{sch} = 40mm$	

TABLE 4.1: Geometric design of the Switched Reluctance Machine

Thus the permeance of a generic flux line is inversely proportional to the length of that flux line. To minimize the unaligned inductance the maximum length of the flux path linking the stator and the rotor poles is considered equal to the flux path along the axis of the stator pole..

4.4.1.1 Region-1 of the Stator-Rotor flux path

For evaluating the SRM's unaligned inductance a linearized machine geometry is considered where the center of the stator tooth lies midway between the two consecutive rotor poles. The pole widths i.e. w_{sp} and w_{rp} are known from the initial sizing and also the the radial distance l_{r1} between the ending tip of the stator pole and the starting tip of the rotor pole can be calculated as follows

$$l_{r1} = \tau_{rp}/2 - w_{sp}/2 - w_{rp}/2 = 11.7mm$$

where $\tau_{rp}/2$ is equal to half of the rotor pole pitch.

As shown in Fig.1 the flux lines of Region-1 originate at the base of the stator pole and

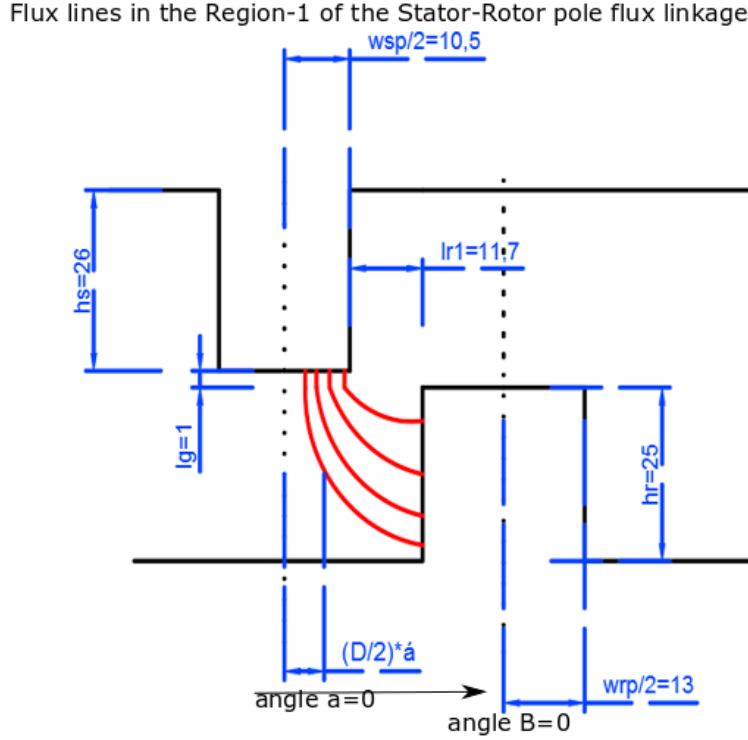


FIGURE 4.3: Plot for the evaluation of the inductance in the region-1[6]

end up at the side of the rotor pole. The angle α is considered as the angle that a flux line subtends at the center of the machine. The radial distance $D/2 * \alpha$ allows us to calculate the respective arc lengths. The length of a flux line at an angle α from the midpoint of the stator tooth can be written as

$$l(\alpha) = l_g + (w_{sp}/2 + l_{r1} - D/2 * \alpha) * \pi/2 \quad (4.10)$$

The above expression is valid within the following angle limits

$$0 \leq \alpha \leq w_{sp}/2$$

4.4.1.2 Region-2 of the Stator-Rotor flux path

The region-2 of the stator-rotor flux path is shown in Fig.2. The flux lines in this case comprise of two arcs in addition to the airgap length. The 1st flux line starts at the side of the stator pole till it's tip while the 2nd flux line starts at the tip of the rotor pole and ends up at it's side. The mathematical relation of the flux line in terms of the two arcs and the airgap is

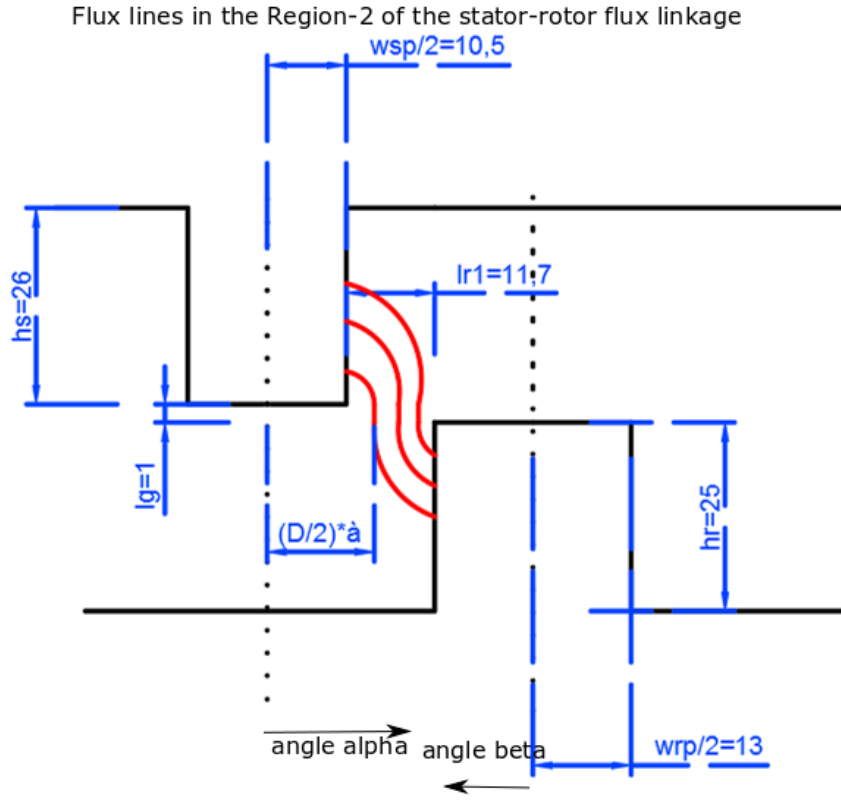


FIGURE 4.4: Plot for the evaluation of the inductance in the region-2[6]

given as

$$l(\alpha) = (D/2 * \alpha - w_{sp}/2) * \pi/2 + l_g + (w_{sp}/2 + lr_1 - D/2 * \alpha) * \pi/2 \quad (4.11)$$

The expression can be simplified to give the following result

$$l(\alpha) = l_g + \pi/2 * lr_1$$

For α varying between the following limits

$$w_{sp}/2 \leq \alpha \leq w_{sp}/2 + lr_1$$

4.4.1.3 Region-3 of the Stator-Rotor flux path

The flux lines in the Region-3 originate from the head of the rotor pole and finish at the side of the stator tooth. The flux lines can be expressed as follows

$$l(\alpha) = \pi/2 * (D/2 * \alpha - w_{sp}/2) \quad (4.12)$$

The above expression is valid within the following angle limits

$$w_{sp}/2 + l_{r1} \leq \alpha \leq w_{sp}/2 + l_{r1} + w_{rp}/2$$

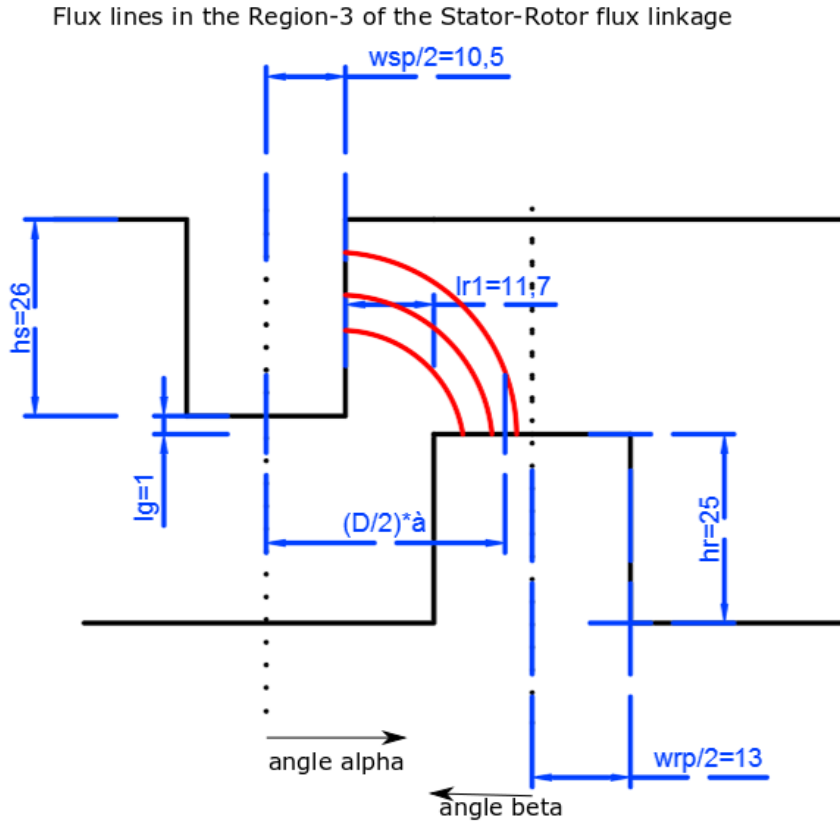


FIGURE 4.5: Plot for the evaluation of the inductance in the region-3[6]

4.4.2 Variation of the unaligned SRM inductance

The unaligned inductance decreases in the Region-1 and increases again in the Region-3 of the flux-linkage plot. While in the region-2 the inductance is a constant. Fig.4.6 shows the plot of the inductance variation with respect to the radial angle between the stator and rotor poles. The minimum value of the unaligned inductance is used to calculate the rotor pole height as evident from the plot.

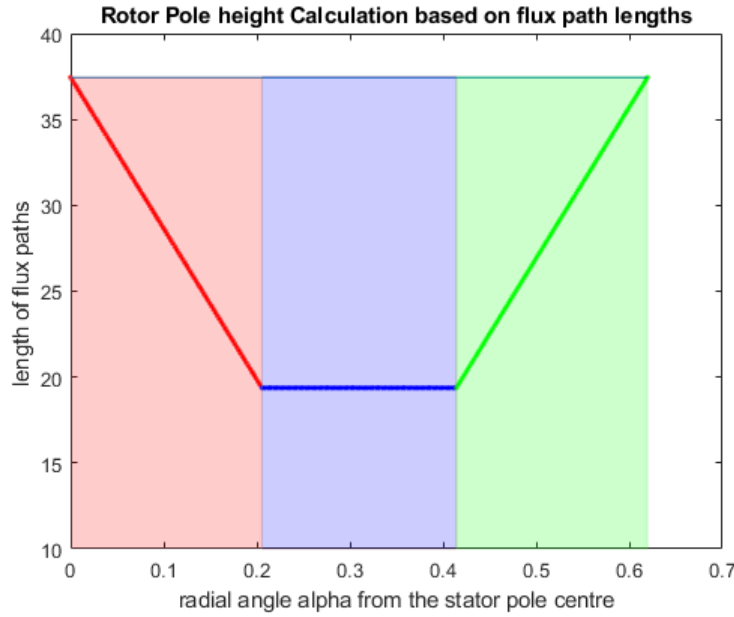


FIGURE 4.6: Variation of flux path lengths with the radial angle[6]

4.5 Performance analysis of Initial Sizing Algorithm

From the known stator pole height and the stator pole width , the copper area can be calculated

$$A_{cu} = FF * h_{sp} * w_{sp} = 69mm^2$$

Considering a single turn winding the peak stator winding current can be calculated from the electrical loading equation

$$i_{pk} = \frac{A_{sp} * \pi * D}{6 * T_{ph}} = 933A$$

The stator slot current density comes out as $13.52A/mm^2$ and it is within the maximum allowable current density of $20A/mm^2$. The current density however exceeds the one chosen during the design parameter selection stage which was $10A/mm^2$. Thus better cooling techniques would have to be employed in order to ensure that the machine sustains a higher current density than the normal in the slot.

Fig.4.7 shows the flowchart of the entire initial sizing algorithm right from inception till the end. The copper area and the peak current are used to calculate the current density which is then checked against the maximum allowable current density in the slot. If the current density exceeds the one that we have chosen, which in our design happens then the Specific electrical loading parameter A_s has to be changed. Since that parameter varies over a dynamic range an attempt will be made in the upcoming chapter to remove that parameter from the design algorithm.

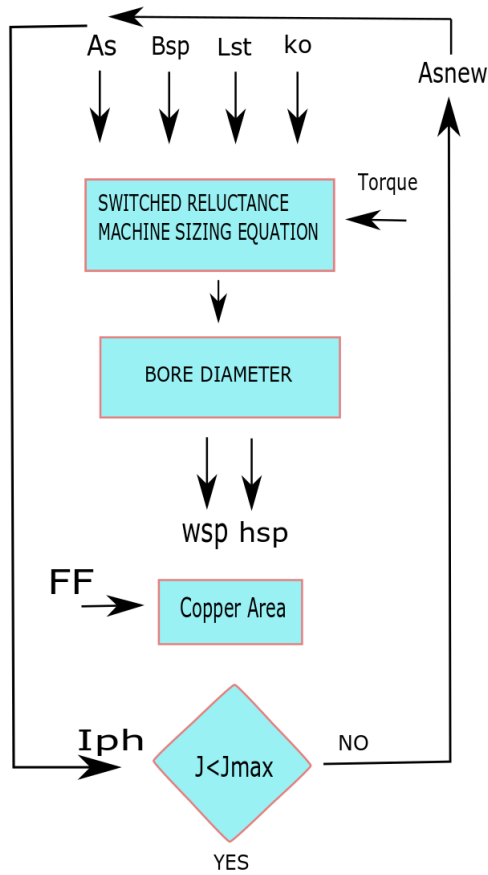


FIGURE 4.7: Initial SRM Sizing Algorithm Flowchart

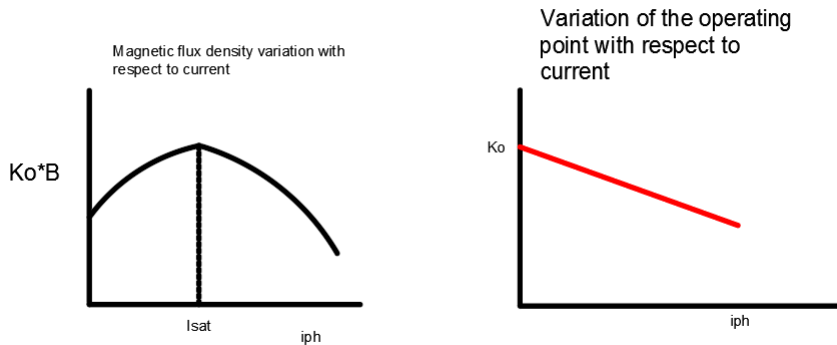


FIGURE 4.8: Effect of the change in excitation current on the operating point[5]

Another problem supposedly with the initial sizing algorithm presented is that the operating point k_o has been assumed constant for all values of the excitation. However in reality the operating point depends on the inductances which are subject to change depending on the levels of the excitation current. Fig.4.8 shows the typical variation of the operating point constant k_o with the current implying a reduction in the torque/Amp level with increasing

levels of excitation.

Chapter 5

Design of SRM using Torque Sizing Equation

5.1 Magnetic Co-Energy Sizing

In this chapter an alternative strategy for the sizing of the SRM is used wherein the machine is analyzed at two different positions of the stator tooth wrt to the Rotor tooth i.e. the aligned and the unaligned position. The two magnetic circuits corresponding to the two geometrical positions are then solved to calculate the flux linkage vs current plots. These in turn help in sizing the machine using the method of magnetic co-energy sizing as discussed below

5.1.1 Calculation of the peak current

To start off a single turn stator winding is assumed. The phase current is expressed in terms of the slot current density chosen, the fill factor and the area of the stator slot. The peak current in the slot can be written as

$$i_{pk} = J_s * FF * A_{ss} \quad (5.1)$$

5.1.2 Calculation of Flux linkages in the aligned position

Since a single turn is assumed the flux linkage with the stator tooth will be expressed as the flux that links with the surface of the pole.

$$\lambda_{as} = A_p * B_{st}$$

$$A_{sp} = D/2 * \beta_s * k_{sp} * D$$

$$\lambda_{as} = D/2 * \beta_s * k_{sp} * D * B_{st} \quad (5.2)$$

With the flux density chosen and the enclosure ratios selected the flux linkages vary as a function of the bore diameter.

5.1.3 Torque Sizing equation

The area enclosed within the Co-Energy loop corresponds to the mechanical energy that can be extracted from the machine per stroke. The increase in the magnetic co-energy from the unaligned to the aligned position can be represented in terms of the peak current and flux linkages as in equ(5.3)

$$\Delta W' = 1/2 * \lambda_{as} * i_{pk} (1 + \sigma_\lambda - \sigma_i - \frac{\sigma_\theta * \sigma_\lambda}{\sigma_i}) \quad (5.3)$$

The design ratios corresponding to the flux saturation and the current saturation had been calculated during the Material selection

$$\Delta W' = 1/2 * [(D/2 * \beta_s * k_{sp} * D * B_{st}) * (i_{pk}) * k_o] \quad (5.4)$$

The mechanical angle corresponding to one stroke can be calculated as follows

$$\Delta\theta = 2\pi/N_{rt}$$

$$T = \Delta W' * m / \Delta\theta$$

5.2 Geometry Calculation

5.2.1 Rotor pole height improvement

For the unaligned inductance calculation in this case the actual rotor geometry is considered. The arc angle subtended in this case will not be $\pi/2$. From Fig.5.1 it can be noticed that the angle θ_1 will equal to the angle subtended by the leading edge of the rotor pole with the line along the axis of the machine.

$$\theta_1 = \pi/2 - (\tau_{rp}/2 - \beta_r/2)$$

$$\theta_1 = \pi/2 - (\pi/4 - \pi/8) = 3\pi/8$$

The Rotor pole height can now be expressed in terms of a radius and an arc angle which in our case equals $3\pi/8$.

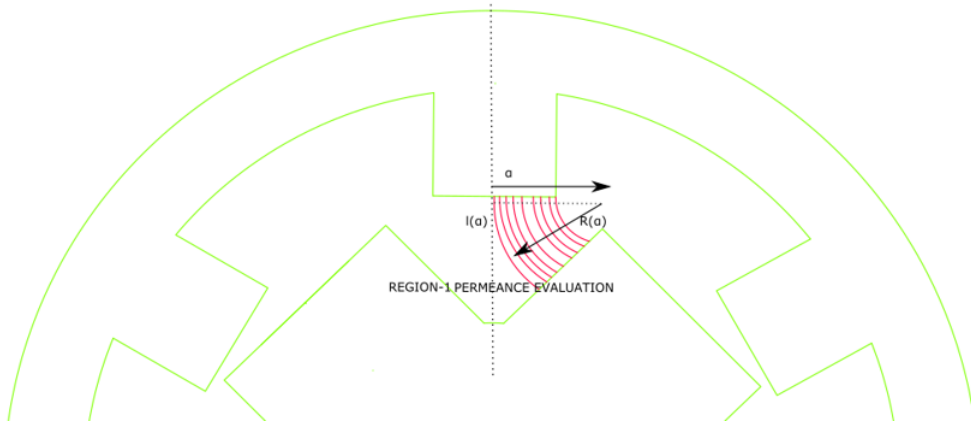


FIGURE 5.1: Actual geometry for the Rotor pole height calculation

5.2.2 SRM Geometrical plots

For the sizing using the magnetic co-energy relations the bore diameter is not evaluated from the output relations but rather the bore diameter is varied within its extremal values starting from zero till the outer diameter. The geometrical parameters are then plotted as a function of the bore diameter as shown in Fig.5.1.

The plots show that for certain values of the bore diameter some geometrical parameters become negative and hence are not feasible. If the bore diameter becomes too small then the shaft diameter becomes negative. On the other hand for higher values of the bore diameter

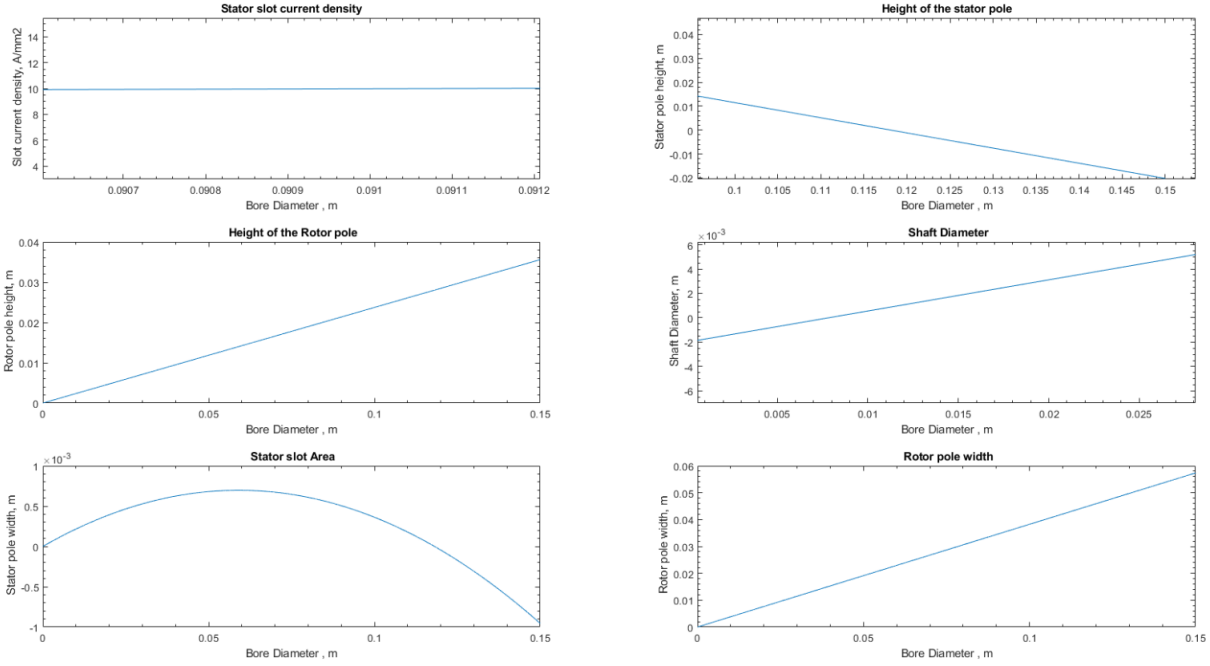


FIGURE 5.2: Geometry plots

the stator pole height becomes smaller and smaller and becomes negative. For the imposed outer diameter constraints of 150mm the minimum and maximum feasible values for the bore diameter are identified as 8mm and 125mm respectively.

5.3 Aligned Magnetic Circuit Calculations

The aligned magnetic circuit of the SRM corresponds to the position when the center of the Rotor axis coincides with the center of the Stator axis. In this case the stator tooth gets saturated as the maximum flux passes through it.

5.3.1 Magnetic Flux density Calculations

To proceed with the calculation of the stator slot current density in the aligned position the flux density distribution in every part of magnetic circuit has to be evaluated. The maximum saturated flux density is assumed in the stator tooth as 1.9T.

$$B_{sp} = 1.9T$$

Knowing the geometrical parameters at first the areas of all the sections of the machine are calculated. For a bore diameter of 91mm and by choosing an aspect ratio of 0.7 we get a stack length of 63mm. knowing these values and the pole arc lengths the cross section are as follows

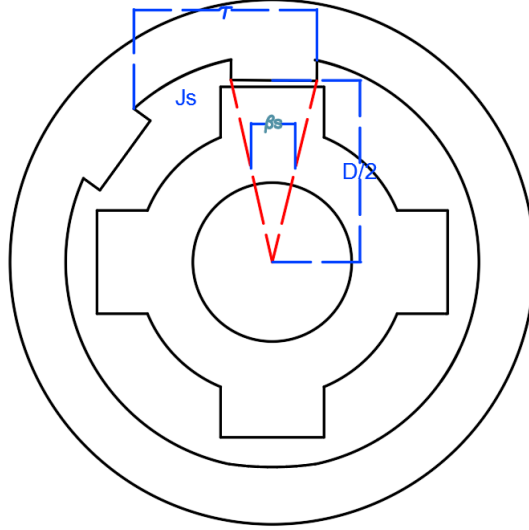


FIGURE 5.3: Stator and Rotor pole enclosures for area calculation

$$A_{sp} = D/2 * \beta_s * L_{st} = 0.0012m^2$$

$$A_{rp} = D/2 * \beta_r * L_{st} = 0.0023m^2$$

$$A_g = \frac{A_{sp} + A_{rp}}{2} = 0.0017m^2$$

$$A_{sy} = b_{sy} * L_{st} = 7.817 * 10^{-4}m^2$$

$$A_{ry} = b_{ry} * L_{st} = 7.817 * 10^{-4}m^2$$

Now by enforcing the flux flowing through the machine the flux densities in the poles and the back iron can be calculated as follows

$$B_{rp} = B_{sp} * (A_{sp}/A_{rp}) = 0.92T \quad (5.5)$$

$$B_{sy} = B_{sp} * (A_{sp}/A_{sy}) = 1.12T \quad (5.6)$$

The Ampere's Circuital law is applied to calculate the stator slot current density by solving the reluctance network shown in Fig.5.4. The reluctances are evaluated by calculating the magnetic permeabilities at various sections of the machine. The reluctance network solution provides a window of bore diameter values for which the slot current density is within the

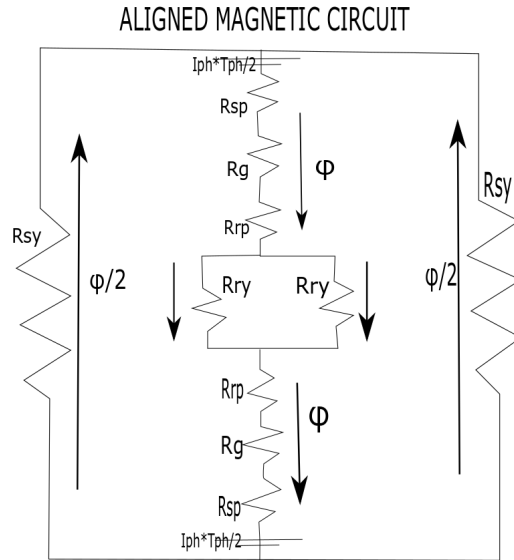


FIGURE 5.4: Reluctance network for the calculation of the slot current density[4]

imposed limits of $10A/mm^2$. Together with the physical limitations of the geometrical parameters the current density requirement reduces the computational effort for the next stage of the algorithm.

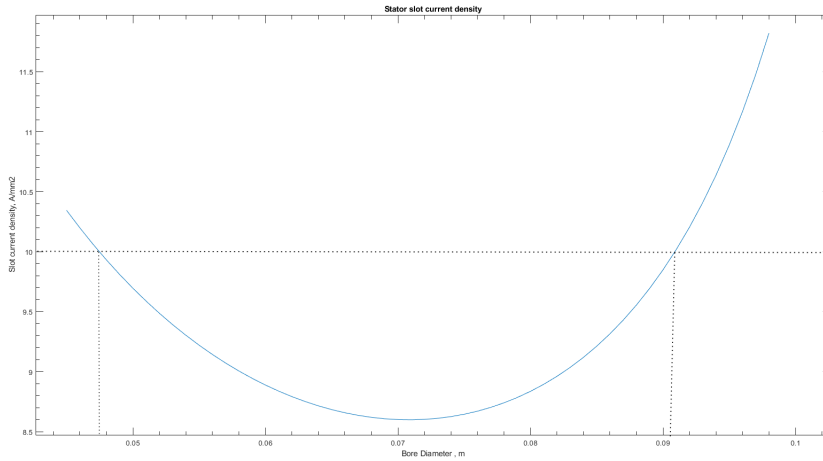


FIGURE 5.5: Stator slot current density feasible values

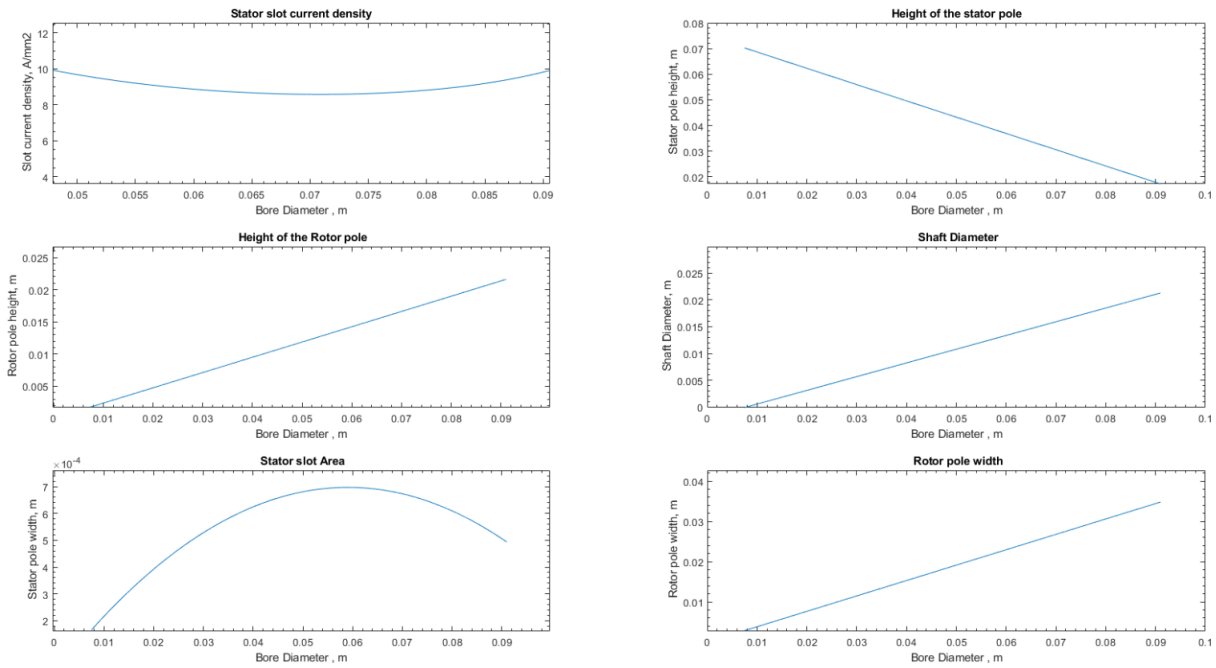


FIGURE 5.6: Geometry plots after eliminating infeasible D values

5.4 Unaligned Magnetic Circuit

The solution of the unaligned magnetic circuit provides the unaligned flux linkage. Since in the unaligned position the pole doesn't get saturated the unaligned inductance doesn't vary with the variation in the current.

However in case of the aligned magnetic circuit saturation plays its role. Fig.5.7 and Fig.5.8 show that the aligned inductances i.e. both the saturated as well as the unsaturated decrease with the increase in the excitation current. Even though the flux linkage also increases with rising current level however the inductance drops as in the saturation region more current is required to magnetize the material.

The unaligned inductance is evaluated by calculating the total permeance of the region through which the flux lines pass while linking the stator with the rotor. The flux linkage plot is divided into three different regions as that illustrated earlier for the rotor pole height calculations.

5.4.1 Area of the Co-Energy Loop

After solving the aligned and the unaligned magnetic circuits the aligned saturated flux linkages are known as well as the unaligned flux linkage values at the peak value of the current. In order to construct the Co-Energy loop another point is needed which is the knee point flux

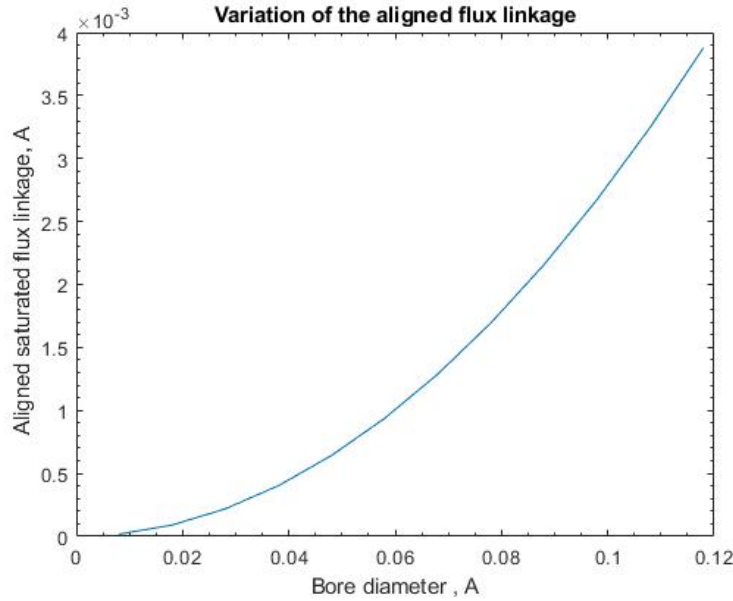


FIGURE 5.7: Plot of the Aligned flux linkage vs the bore diameter

linkage value. That information is known from the magnetization BH curve plots.

Fig.5.9 and Fig.5.10 show the construction of the magnetic Co-Energy plot. The area $\Delta W'$ in Fig.5.9 shows the increase in the Co-energy area loop. The increase in the Co-Energy area loop is proportional to the Torque that can be extracted from the machine and hence it is quite important in the performance analysis of SRM drives.

The Saliency ratio drops as the bore diameter value increases. The increase in the bore diameter causes a reduction in the stator pole height. As the pole height shrinks a higher level of current is required to be injected so that the same current density can be maintained. Higher current levels then cause the inductance to saturate and the Saliency drops which in turn causes the torque output of the machine to decrease. Fig.5.12 shows the Saliency plot for the 6/4 SRM of our design. The magnetic co-energy sizing technique thus lets us have an intuitive idea about the inner workings of the machine and gives a better chance of predicting the machine's performance.

5.4.2 Magnetic Co-Energy Sizing Algorithm

Fig.5.11 sums up the steps taken in order to size the machine using the torque sizing equations. The aligned magnetic circuit provides the slot current density and the flux linkages. Also it imposes a maximum value of the bore diameter for the succeeding block of the unaligned magnetic circuit. The unaligned magnetic circuit gives the unaligned flux linkages. Taken

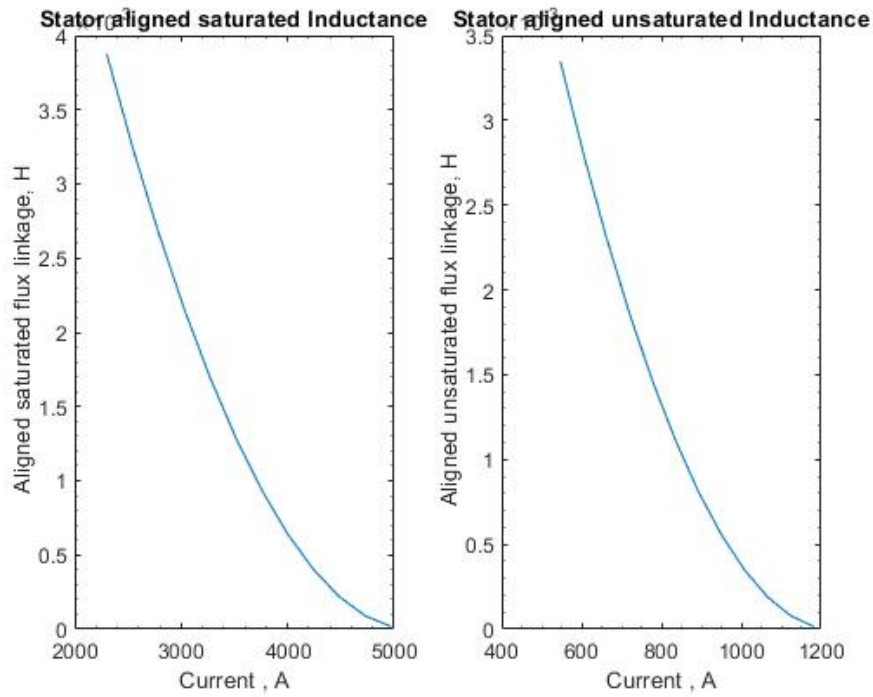


FIGURE 5.8: Aligned inductances variation with excitation

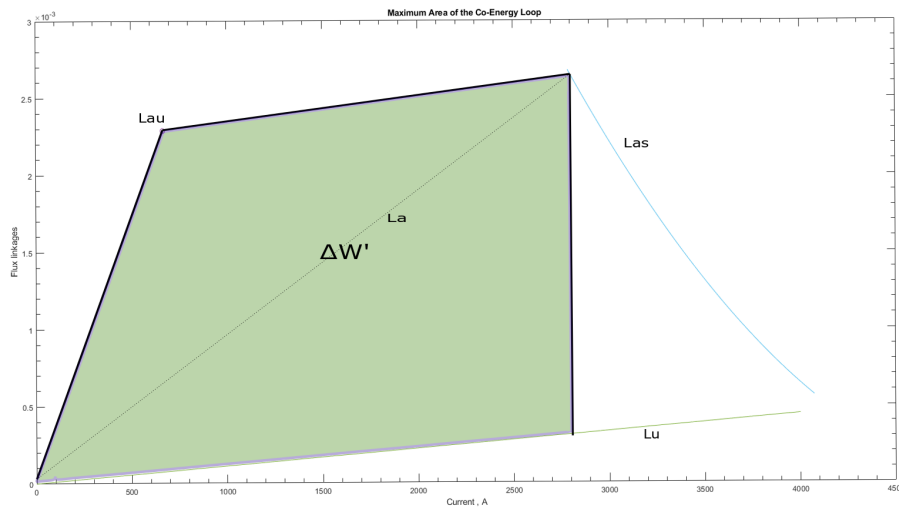


FIGURE 5.9: Area of the Co-Energy Loop calculated

together the flux linkages are used to set up the co-energy loop of the SRM. The remaining stage is the finite element validation which will be taken up in the next chapter.

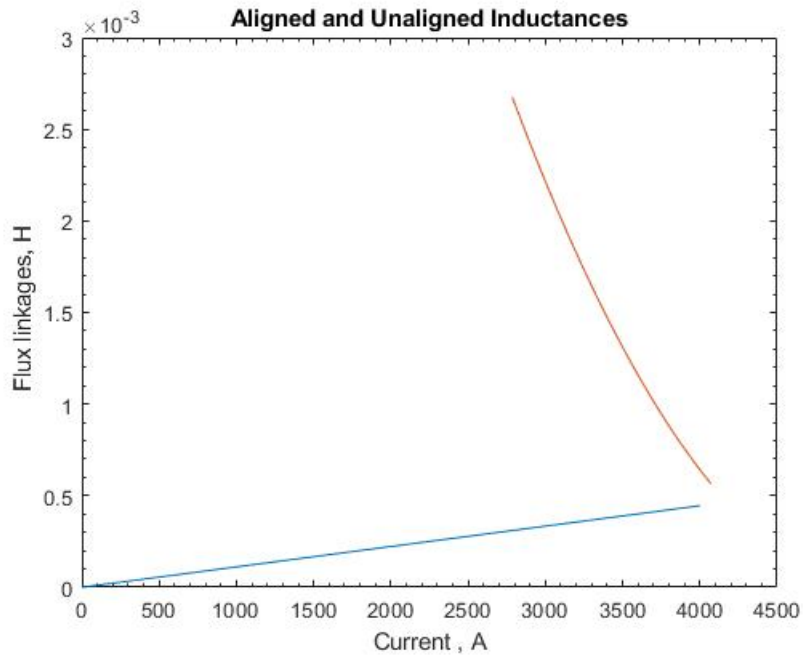


FIGURE 5.10: Unaligned inductance and aligned saturated inductance variation with the current

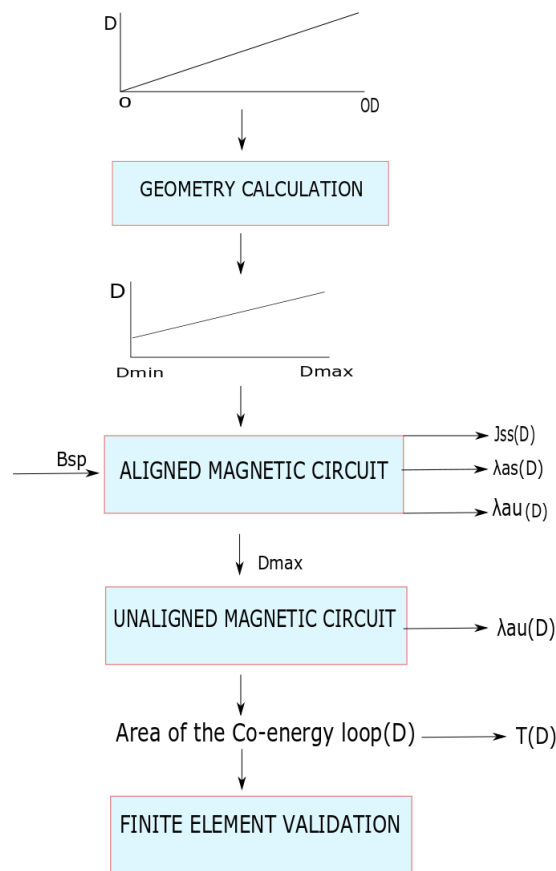


FIGURE 5.11: Flowchart of the Magnetic Co-Energy Sizing Algorithm

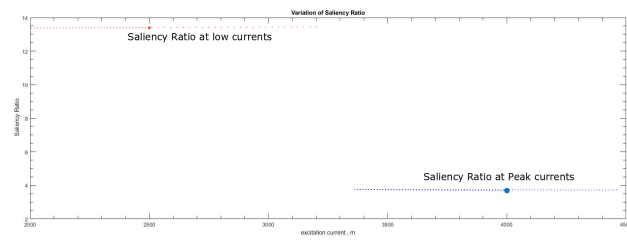


FIGURE 5.12: Variation of Saliency Ratio with the excitation current

Chapter 6

Conclusions and Results

In this chapter finite element analysis is taken up for the analytical design completed in the previous section. At first the geometry is designed in FEMM software by setting up the properties as those selected for the analytical design. Steady State analysis as well as transient analysis will be taken up in this chapter. Lastly a comparison will be done with the analytical model based on the results of the transient analysis.

6.1 Steady state analysis of SRM using FEA

The designed FEM SRM geometry in the aligned position is shown in Fig.6.1. A single phase is excited at a time which sets up a flux in the machine. According to the Fig.6.1 the stator tooth is clearly the most highly saturated and the obtained value of the flux density is equal to the saturated flux density value obtained during the analytical modelling stage.

Fig.6.2 shows the SRM in the unaligned position and the flux density values are not saturated for the stator tooth since the flux now has to pass through the large airgap before it can link with the rotor tooth. Further the effect of fringing is quite considerable when the SRM is in the unaligned position. Therefore the value for the unaligned inductance obtained from the analytical means and those evaluated by FEA analysis has an error of 25 %. However referring to the Magnetic Co-Energy plot in Fig.5.9 we can observe that even if the L_u point is displaced by an error of around 20% the overall area of the Co-Energy loop doesn't change significantly.

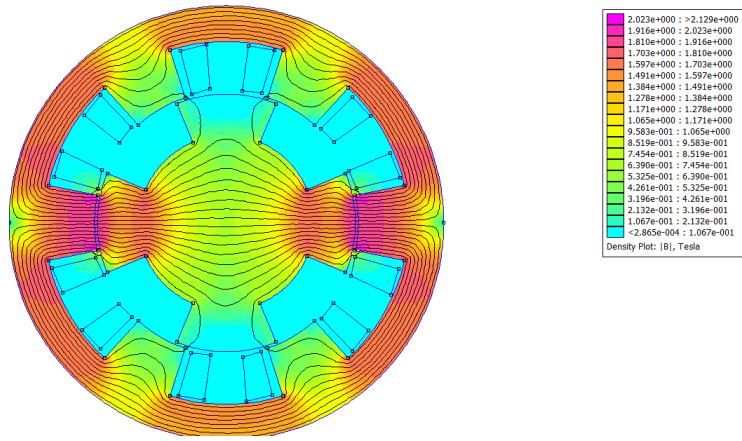


FIGURE 6.1: FEA analysis of 6/4 SRM in the aligned position

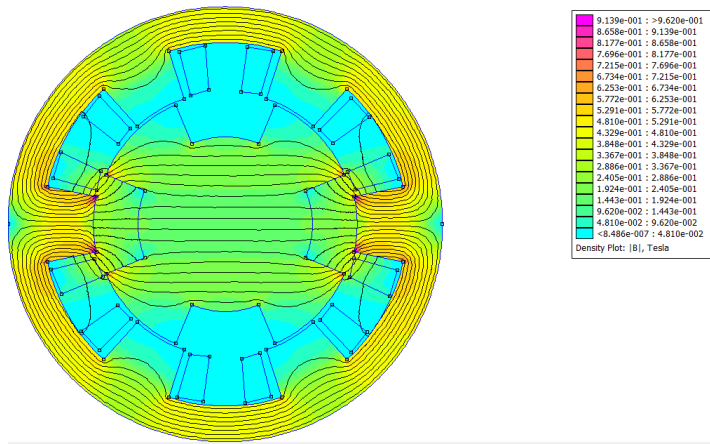


FIGURE 6.2: FEA analysis of 6/4 SRM in the unaligned position

6.2 Transient Analysis of SRM using FEA

For constructing the flux linkage vs current plot of the SRM in the aligned position a transient FEM 2D simulation run is required. Starting from an excitation of 0A the current is increased and the SRM machine model is solved at discrete points of the excitation current.

Fig.6.3 till 6.6 show the FEM transient simulation results at discrete excitation levels of 10, 500, 1200 and 2950 A respectively. The resulting flux density points vs the excitation current are plotted in Fig.6.7 and interpolated to get the saturated flux density values in the whole range from 0 till the peak current. To improve the efficiency of the algorithm the number of transient simulation runs can be increased. This however makes the algorithm more computationally expensive.

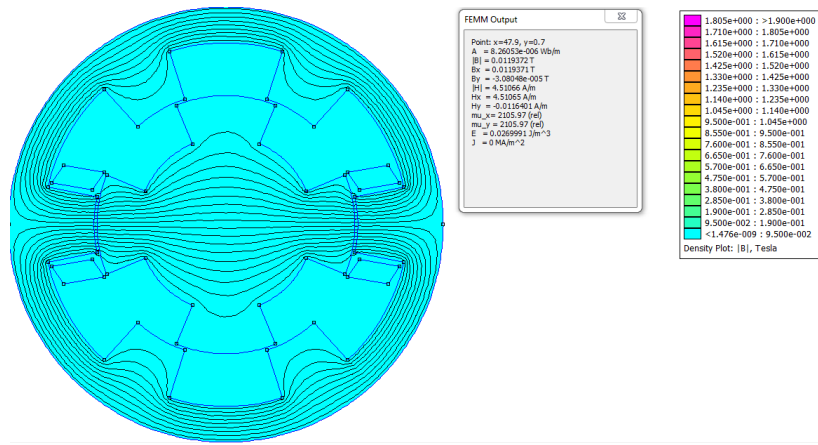


FIGURE 6.3: FEM aligned transient analysis with an excitation of 10 A

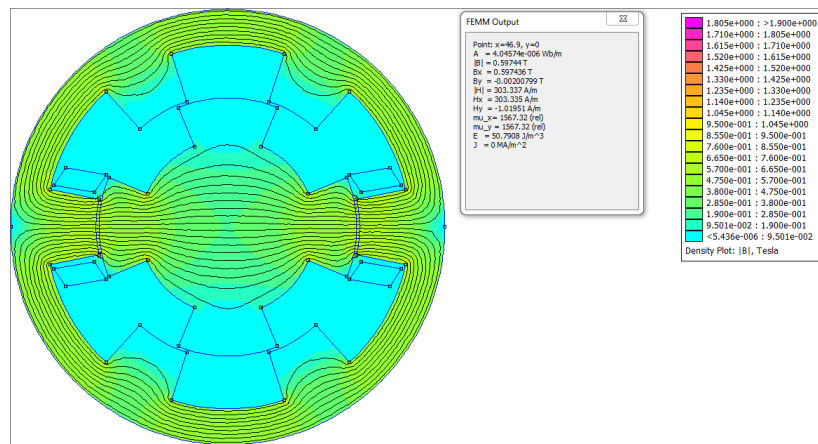


FIGURE 6.4: FEM aligned transient analysis with an excitation of 500A

6.3 Results discussion

The FEM obtained simulation results along with the analytically obtained results are shown in Fig.6.8. Some observations about the resulting design are as follows

1. The analytically obtained flux linkage vs current plot requires the approximation of the curvilinear trajectory in terms of two different slopes. However the actual magnetic material doesn't exhibit such a subtle changing from the unsaturated condition to the saturation region.
2. The Finite element obtained results show that indeed the actual aligned inductance trajectory bears a close resemblance with the actual curvilinear path
3. The knee point value calculation for the analytical results gave a higher value of B_{kn} as compared to the simulated finite element simulation results

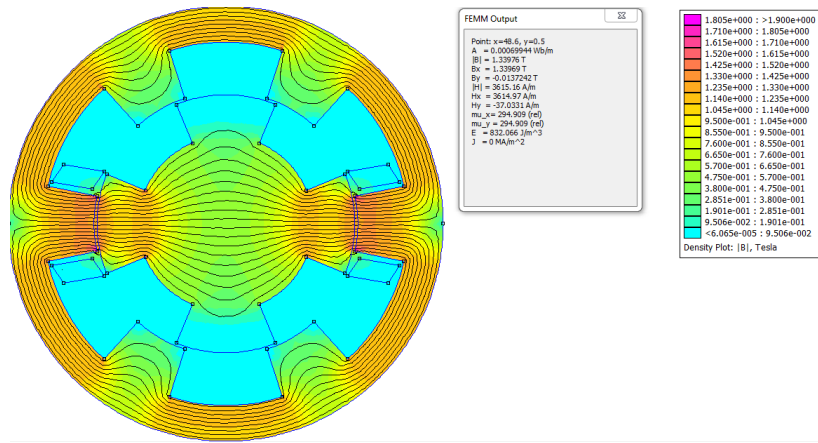


FIGURE 6.5: FEM aligned transient analysis with an excitation of 1250 A

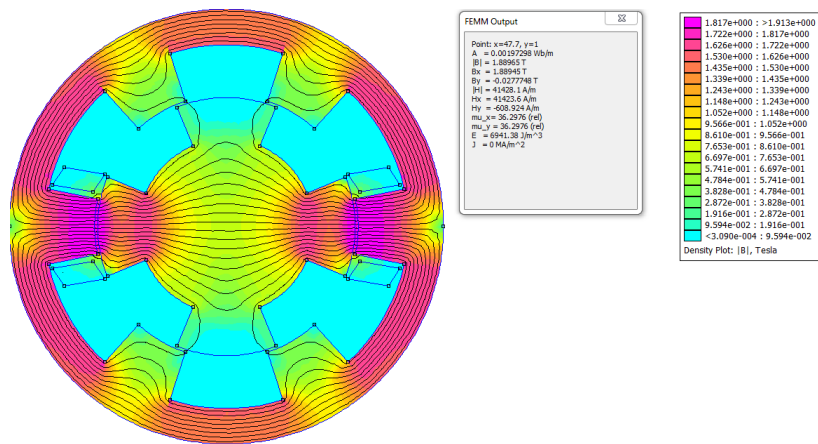


FIGURE 6.6: FEM aligned transient analysis with an excitation of 2950A

4. This implies that in the analytical calculations we were somewhat overestimating the torque that could be extracted from the drive.
5. The unaligned flux linkage point is also different with the two methods and an error of around 20% is observed.
6. In order to extract the same amount of torque the stack length of the machine has to be increased

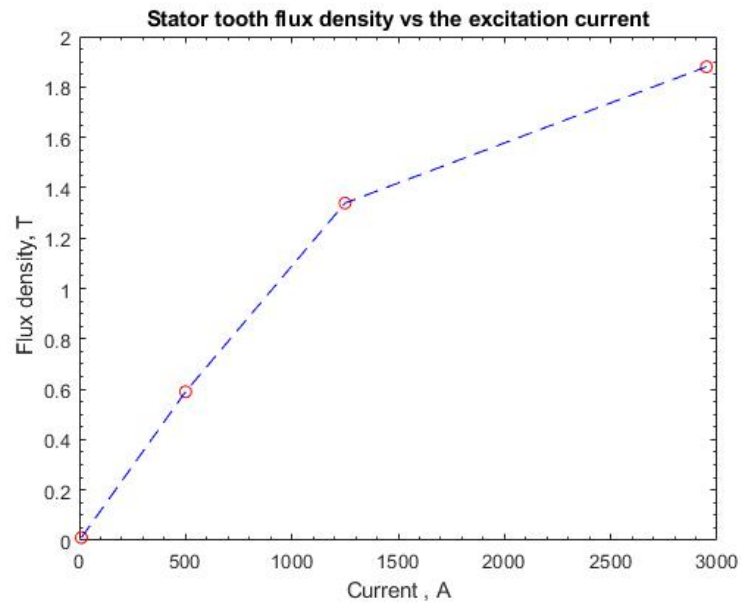


FIGURE 6.7: Plot of Stator tooth flux density in a transient analysis

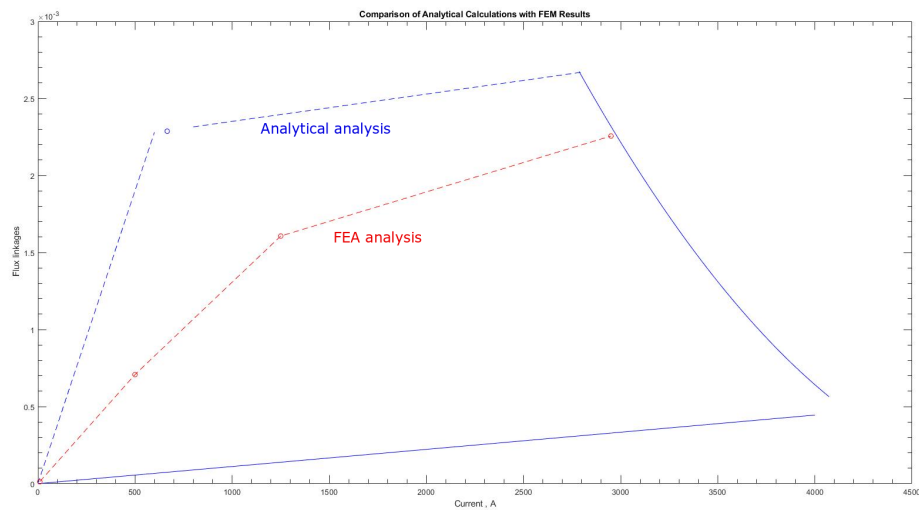


FIGURE 6.8: Comparison of Flux linkage plot calculated by Analytical and FEM methods

Appendix A

Magnetic Material Data Sheet

<https://cogent-power.com/cms-data/downloads/Cogent%20NO%20brochure%202016.pdf>

Bibliography

- [1] Vk Mehta and Rohit Mehta. *Principles of Electrical Machines*, S.CHAND COMPANY LTD, 2008.
- [2] *Advanced AC Machines lectures*, The University of Nottingham, .
- [3] TJ MILLER. *Electronic Control of Switched Reluctance Machines*.
- [4] Krishnan Ramu. *Switched Reluctance Motor Drives Modeling, Simulation, Analysis, Design, and Applications*, INDUSTRIAL ELECTRONICS SERIES, 2001.
- [5] *National Programme on Technology and enhanced learning NPTEL Lectures on Switched Reluctance Machines*, .
- [6] V Radun. *Comprehensive Design Methodology for Switched Reluctance Machines*, IEEE Xplore, 2001.